ornl

OAK RIDGE NATIONAL LABORATORY

LOCKHEED MARTIN

MANAGED AND OPERATED BY
LOCKHEED MARTIN ENERGY RESEARCH CORPORATION
FOR THE UNITED STATES
DEPARTMENT OF ENERGY

ORNL-27 (3-96)

ORNL/TM-13750

Developing A CD-CBM Anticipatory Approach For Cavitation – Defining A Model-Based Descriptor Consistent Across Processes

Phase I Final Report
Context-Dependent Prognostics and Health Assessment:
A New Paradigm for Condition-based Maintenance
SBIR Topic No. N98-114

Glenn O. Allgood
Stephen W. Kercel
William B. Dress Jr.

DISCLAIMER

DISCLAIMER

Portions of this document may be illegible in electronic image products. Images are produced from the best available original document.

ORNL/TM-13750

Instrumentation and Controls Division

DEVELOPING A CD-CBM ANTICIPATORY APPROACH FOR CAVITATION – DEFINING A MODEL-BASED DESCRIPTOR CONSISTENT ACROSS PROCESSES

Phase I Final Report
Context-Dependent Prognostics And Health Assessment:
A New Paradigm For Condition-Based Maintenance
SBIR Topic No. N98-114

Glenn O. Allgood
Stephen W. Kercel
William B. Dress Jr.

Date Published—June 1999

Prepared by the
Oak Ridge National Laboratory
Oak Ridge, Tennessee 37831-6202
Managed by
LOCKHEED MARTIN ENERGY RESEARCH CORP.
For the
US DEPARTMENT OF ENERGY
Under contract DE-AC05-96OR22464

CONTENTS

LIST OF FIGURES

Objective

The object of this research, and subsequent testing, was to identify specific features of cavitation that could be used as a model-based descriptor in a context-dependent condition-based maintenance (CD-CBM) anticipatory prognostic and health assessment model. This descriptor is based on the physics of the phenomena, capturing the salient features of the process dynamics. The test methodology and approach were developed to make the cavitation features the dominant effect in the process and collected signatures. This would allow the accurate characterization of the salient cavitation features at different operational states. By developing such an abstraction, these attributes can be used as a general diagnostic for a system or any of its components. In this study, the particular focus will be pumps. As many as 90% of pump failures are catastrophic. They seem to be operating normally and fail abruptly without warning. This is true whether the failure is sudden hardware damage requiring repair, such as a gasket failure, or a transition into an undesired operating mode, such as cavitation. This means that conventional diagnostic methods fail to predict 90% of incipient failures and that in addressing this problem, model-based methods can add value where it is actually needed.

An important element of CD-CBM is the development and formulation of the extended process feature vector (*fv*). This model-based descriptor encodes the specific information that describes the phenomena and its dynamics and is formulated as a data structure consisting of several elements. The first is a descriptive model abstracting the phenomena. An example would be a chirped-exponentially decaying sinusoid—the model from this study characterizing cavitation. The second is the parameter list corresponding to the functional model. Using the elements of the cavitation model, the list would include frequency, decay rate, and chirp rate. The third is a figure of merit. A single number between 0 and 1 [0,1] representing a confidence factor (probability measure) that the functional model and parameter list actually describes the observed data. For a given location in a given flow loop, these data structures will be different in value but not content. The feature vector is formulated as follows: *fv* => [<f(x,t,)>, {parameter list}, confidence factor]. [Note: This is a much more general concept of a vector than the popular comma-delimited list of numbers.]

An example using the results from this study is

$$fv \Rightarrow [\langle e^{-\gamma t}\cos(\omega t\kappa+\alpha\kappa^2t^2),\ e^{-\gamma t}\sin(\omega t\kappa+\alpha\kappa^2t^2)\rangle, \{\omega=0.008,\ \gamma=0.0056,\ \alpha=-0.0009\},\ cf=0.80]. \quad (1)$$

As stated earlier, this project demonstrates a model-based approach to the characterization and detection of impending (or incipient) cavitation, which can lead to catastrophic failures in pumps. Catastrophe is used in the mathematical sense. A system experiences a catastrophe when it abruptly changes, or bifurcates, to a fundamentally different state. Some catastrophes are reversible, such as cavitation, and can be remedied by changing the operating point of the system. Others are irreversible, such as bearing failure, damaging the system and requiring the repair and replacement of elements and possibly the component itself.

A reversible catastrophe was examined in this experiment. The reason for this is obvious; the same catastrophe could be repeated to ensure the statistical significance of the data. From these, the descriptor for impending (it is about to happen) or incipient (it just started happening) catastrophic cavitation could be identified. The key in the experimental approach is that the same model-based strategy that detects incipient reversible catastrophes should work for irreversible catastrophes as well. The technique is to identify the nonlinear differential equation that underlies the process, locate its bifurcation point, and observe the proximity of the present operating point to it. An added benefit from this approach is that the data can be collected without destroying equipment or the flow loop.

Formulation

Bayesian analysis is the most effective method for extracting the useful information (process feature vector) from the experimental data. It should be noted that the differential equation describing a process can be obtained directly through Bayesian analysis of experimental data and has more utility than the function that solves the differential equation. The differential equation is much more than a "curve-fitted" estimate of a function. The processes of interest are nonlinear and often do not have a solution in closed mathematical form. For example, consider the

Lorenz equations. The solution is a function of applied energy, viscosity and several other things. The behavior is highly periodic at low energy. As energies increase, the system becomes chaotic. There is no closed form function that describes this behavior. However, the entire description is subsumed in the system of differential equations. The bifurcation point can be deduced from several of the parameters of the equations and the present operating point can be determined from observed data. All this can be done with no description of the solution except the observation that it is whatever function happens to solve the system of equations.

The direct deduction of the differential equation is future task. This work was limited to obtaining a functional form that constitutes an approximate solution of the differential equation, the parameters corresponding to the function, and the probability that the analysis has led to the right answer.

Previous Work

There are a variety of sensors and their associated measurements that are used in predictive maintenance of mechanical systems. The three most popular are tribology, vibration analysis, and thermography. All three are quite mature from the perspective that economical and reliable sensing elements and systems are commercially available. However, there are questions on the capability of these sensors to provide accurate measurements and estimates of cavitation. It seems they exploit only a small fraction of the information contained in the data. Given this, the test plan focused on using acoustic emissions (AE) measurements to extract the characterizing features of cavitation. The following is a short description on the limitations of using tribology, vibration analysis, and thermography to discern cavitation.

Tribology

Strictly speaking, tribology is the study of rubbing surfaces. Informally, in the predictive maintenance community, tribology is the term used for the analysis of metal particles in oil. The idea is that by analyzing for particulates, effects such as bearing wear can be deduced. One of the problems with this approach is that it is not a good diagnostic of incipient failure.

Vibration Analysis

Vibration analysis is also very popular in condition monitoring of mechanical systems. A major problem with vibration analysis is that practically everything occurring in a pump adds a component to the vibration pattern. A major unsolved problem, then, is the extraction of the signature of a specific effect from the other vibration mechanisms occurring at the same time. Spectral analysis attempts to deal with this problem, but real-world effects are seldom described by isolated sinusoids.

Thermography

Thermography is the imaging of the heat pattern generated by a mechanical system. The argument is that if the system is not operating normally, it will generate hot spots. The advantage of thermography is that it depends on infrared detection and can be done at a standoff, without touching the machine being tested. One shortcoming with thermography is that heat transients are comparatively slow and there is a substantial time delay between a change in the internal condition of a pump and the emergence of a hot spot at the exterior. This is very undesirable for a sensor to be used for detection of incipient catastrophic failures.

Rough Heuristics

Sensor technologies for condition monitoring are fairly mature. The problem resides in the analytic approaches and methodologies applied to the analysis on the collected data. In some instances, they are simply presented to an operator or maintenance expert for subjective interpretation. Often, simple threshold detection is used. If a certain measurement goes out of range, the machine is taken out of service whether there is really anything wrong with it or not. A slightly more sophisticated approach is to use trend analysis. This is based on the idea that if the machine keeps doing what it has been doing, then its future state is predictable. The problem with this reasoning is that some 60%-80% of the problems associated with a system are not time related but event driven. The mission and goal and its mapping onto the operational state of the system dictates the true remaining life of the system.

The fallacy with these approaches is that pumps do not keep doing what they have been doing. Pumps and pump components seldom wear out and the state of a pump does not gradually evolve to failure. Almost all pump failures are catastrophic; pumps abruptly start doing something very different from what they had been doing. This is the type of failure an impending failure detection scheme must accurately predict.

Model-based Analysis

Conventional signal analysis is based on simple curve fitting and trending of vibration data. This is insufficient for several reasons. First, it discards most of the information generated by the sensor. Second, it makes important control and system operational decisions based on extrapolation. This will not meet the optimization demands since it is well known that catastrophic pump failures occur frequently in practice and are not predicted by extrapolation. There are other anecdotes that support this premise. One manager in the aerospace industry has stated that 85% of aircraft component failures are event driven, i.e., the failures occur in context with what the aircraft has been asked to do in order to meet mission needs and has nothing to do with time itself. Greene and Casada note that the testing procedures themselves can lead to pump failure.[3] This indicates the need for anticipatory measurements.

Another widely used method of signal processing is Fourier-based spectral analysis.[1,2] This is completely inappropriate for pump signature analysis. Acoustic signatures of defective pumps are highly non-stationary and Fourier analysis averages out the interesting features. It is also noteworthy that in their discussion of modeling, they limit themselves to linear modeling. It is true that nonlinear models are more difficult to identify, however, nonlinear models contain the information needed to anticipate catastrophes.

It seems that model-based analysis is completely unknown in the conventional practice of predictive or condition-based maintenance (CBM). This was highlighted at a National Institute of Standards and Technology (NIST) workshop on CBM (November 17, 1998) where it was identified as one of three major research areas for CBM. Williams, et al., have identified some of the advanced methods currently being used.[3] As an example, they note that neural networks are completely unsuitable for CBM. In their words: "The field of neural nets is growing rapidly and is likely to yield useful results in the future but there is an element of 'use it and see' about it." It is clear that Williams, et al. are completely unaware of wavelet and Gabor analysis or what it could do for CBM. They show that key acoustic diagnostic features are inherently non-stationary and see the need for something like multi-resolution analysis. Many of the processing tricks they discuss could be more easily and effectively done by wavelet analysis.

State-of-the-art diagnostic systems are based on trending, spectral analysis, and expert systems. Remarkably, Dalhousie University, the home of formal Anticipatory System Theory, gives a professional course on Predictive Maintenance Technology Awareness Training.[4,5] The syllabus for March 1998 made absolutely no mention of anticipatory systems for predictive maintenance.

Features of Impending Cavitation (Theory)

If cavitation started when the minimum flow pressure dropped below the vapor pressure of the liquid, the prediction of the inception of cavitation would be straightforward. However, many physical effects cause the actual inception point to be further from that predicted by this criterion. One of the most troublesome is the effect of surface tension at a nucleation site. Since the liquid can withstand tensions below the vapor pressure, this has to be taken into account. A microbubble of radius, R_N, and surface tension, S, containing only vapor, is in equilibrium if the liquid pressure is $p = p_V - 2S/R_N$. The liquid pressure must fall below this critical point for cavitation to start. Unfortunately, the liquid contains several nucleation sites having several radii. These vary with the physical situation and the quality of the fluid.[6] Therefore, the onset of cavitation and its precursors must be observed directly.

One approach is to obtain the nuclei number distribution function, $N(R_N)$, such that $N(R_N)dR_N$ is the number of nuclei per unit volume with radii between R_N and $R_N + dR_N$. The problem with this approach is that there is no straightforward way to measure the nuclei distribution.[7] [As an aside for a topic of future experimental research, it may be worth considering using AE-based technologies to measure this distribution function.]

Air can cause cavitation. Dissolved air will contribute to the partial pressure of the cavitation bubble. As the bubble moves to a region of higher pressure, the vaporized liquid will condense, leaving the air bubble remaining. Air is slow to redissolve.[7] Thus, one of the things that can go wrong with a cavitation experiment in a test loop is that the air bubbles from the first pass are not redissolved in the loop. The return leg of the test loop must be long enough and at high enough pressure for the air bubbles to become reabsorbed. Otherwise, the number of nucleation sites will grow rapidly as the experiment runs. It should be noted that cavitation inception data taken without bubble population data are practically useless. Total air content provides a good estimate of bubble population. The bubble population typically increases with total air content.[8]

There are several other effects that contribute to resolving the complexity of cavitation.[9] The first is residence time. The cavitation bubble takes a finite time to form. Residence time depends on pump size, flow rate and temperature, but if the cavitation nucleus is in the region of low pressure for less than the residence time, the bubble will not form. This has the effect of lowering the critical cavitation number. Turbulence causes localized low pressure, significantly below the mean pressure of the flow and is often the site of incipient cavitation. This effect is dependent on the Reynolds number, but is a separate effect from the dependency of the pressure coefficient on the Reynolds number. Turbulence has the effect of raising the critical value of the cavitation number. Surface roughness also creates localized low-pressure perturbations. Localized low pressure is a departure from the widely used simplifying assumption that pressure is uniform at an average value through a cross section of the stream.

Due to various effects, a pump will have its minimum cavitation inception number at its design flow rate.[10] In the experiment, there is a need to run the flow loop driver pump near its design flow rate to minimize pump cavitation. Even after the pump cavitation bubbles collapse, their residual air bubbles will remain and could lead to excessive nucleation sites in the venturi chamber.

Practically everything that can be said about the properties of the cavitation bubble is based on the Rayleigh-Plesset equation.[11] To find a solution for the equation is difficult. It is probably more computationally efficient to try to use Bayesian methods to do a direct estimate of the coefficients of this nonlinear differential equation than to try to estimate parameters for its various approximate solutions. The generalized differential equation gives the instantaneous bubble radius, R(t), in response to the driving pressure far from the bubble, $p_\infty(t)$.

$$\underset{(1)}{\frac{pv(T_\infty)-p_\infty(t)}{\rho_L}}+\underset{(2)}{\frac{pv(T_B)-pv(T_\infty)}{\rho_L}}+\underset{(3)}{\frac{p_{Go}}{\rho_L}\left(\frac{T_B}{T_\infty}\right)\left(\frac{R_o}{R}\right)^3} \qquad (2)$$

$$=\underset{(4)}{R\frac{d^2R}{dt^2}}+\underset{(5)}{\frac{3}{2}\left(\frac{dR}{dt}\right)^2+\frac{4\nu_L}{R}\frac{dR}{dt}}+\underset{(6)}{\frac{2S}{\rho_L R}}$$

The equation is derived based on several simplifying assumptions that turn out to be reasonable in practice. It assumes a single spherical bubble in an infinite liquid domain whose remote temperature, T_∞, is constant in time. There is no uniform heating of the liquid due to radiation or internal heating. Liquid density, ρ_L, is assumed constant. Dynamic viscosity, μ_L, is assumed constant and uniform. The bubble contents are homogeneous and the temperature, $T_B(t)$, and pressure, $p_B(t)$, inside the bubble are independent of location. It is also assumed the bubble contains a contaminant gas with a partial pressure, p_{Go}, given a reference bubble radius R_0, and temperature, T_∞, and that there is negligible mass transfer between the liquid and the contaminant gas.

The driving term depends on the pressure in the liquid far from the bubble, $p_\infty(t)$. The remote vapor pressure of the liquid, $p_vT(_\infty)$, depends only on the liquid and the remote temperature. The liquid density is a property of the liquid. The second term is the thermal term. If thermal effects are to be neglected, then $T_B(t) = T_\infty$, and $p_v(T_B)-p_v(T_\infty) = 0$. When this term is non-zero, it can greatly affect the growth rate of the bubble. The fifth term depends on the kinematic viscosity of the liquid, ν_L. The sixth term depends on the surface tension of the liquid, S.

A consequence of the Rayleigh-Plesset equation is bubble instability. If the bubble radius is greater than a critical radius, any small perturbation in pressure will cause it to grow without bound. The critical radius is approximately

$4S/3(p_v-p_\infty)$. As the pressure, p_∞, drops, the critical radius drops, which means that more nuclei in a given distribution are induced to cavitate. This is why there is a rapid increase in the number of visible bubbles in a cavitating flow as the pressure drops.[12]

In the most simplified case, the solution of the Rayleigh-Plesset equation will lead to an oscillating response in which the contracting part of the bubble represents a catastrophic collapse. In reality the oscillation does not occur. As the bubble approaches zero radius, it becomes unstable to nonspherical perturbations; it shatters into a cloud of even smaller bubbles during the first collapse. This generates powerful shock waves that produce AE.[13] The cloud will then expand and collapse and this will also produce powerful shock waves.[14]

The collapse of a bubble near a hard surface produces a microjet directed toward the hard surface and then a collapsing bubble cloud. Due to its high, local pressure, the microjet emits noise and causes damage. The collapsing remnant bubble cloud causes even more noise and damage than the microjet, although the mechanism by which it does so is not understood.[15]

The natural frequency at which an isolated bubble oscillates in a quiescent liquid can also be determined from the Rayleigh-Plesset equation.[16] This suggests the natural frequency should be between 10 kHz and 1 MHz. Acoustic pressure varies as a second derivative of bubble volume.

$$\omega_P = \left[\frac{3(\bar{p} - pv)}{\rho_L R_E^2} + \frac{4S}{\rho_L R_E^3} - \frac{8\nu^2}{R_E^4} \right]^{\frac{1}{2}} \tag{3}$$

For an isolated bubble, the second order nonlinear effects have been determined by Kumar and Brennen.[17] The nonlinear differential equation is Equation 4. The solution is Equation 5, as clarified by Equations 6–9. This may be a crude model for a first try at Bayesian estimation. The bubble radius will oscillate at integral harmonics of the excitation, if the excitation is a remote pressure, oscillating at a single harmonic frequency. Because the response goes inversely with the order of the harmonic, only the first 50 harmonics contribute to the response. For weak excitation, this model tracks fairly well with a direct numerical solution of Equation 4. More accurate solutions appear in the literature, but this one is easily extended to bubble clouds.

$$R\frac{D^2R}{Dt^2} + \frac{3}{2}\left(\frac{DR}{Dt}\right)^2 + \frac{4\nu}{R}\frac{DR}{Dt} + \frac{2S}{\rho R} = \frac{P_v - P_x(t)}{\rho} + \frac{P_{g0}}{\rho}\left(\frac{R_0}{R}\right)^{3k} \tag{4}$$

$$\frac{P_n}{\omega_b^2 R_0^2} = \Lambda(n)\frac{R_n}{R_0} + \sum_{j=1}^{n-1} \beta_1(n,j)\frac{R_j}{R_0}\frac{R_{n-j}}{R_0} + \sum_{j=1}^{N-n} \beta_2(n,j)\frac{\bar{R}_j}{R_0}\frac{R_{n+j}}{R_0} \tag{5}$$

$$\omega_b = \left(\frac{3kP_{g0}}{\rho R_0^2} - \frac{2S}{\rho R_0^3}\right)^{\frac{1}{2}} \tag{6}$$

$$\Lambda(n) = \left[\frac{n^2\delta^2}{\omega_b^2} - 1 - i\frac{n\delta}{\omega_b}\frac{4\nu}{\omega_b R_0^2}\right] \tag{7}$$

$$\beta_1(n,j) = \frac{3k+1}{4} + \frac{3k-1}{2}\frac{S}{\rho\omega_b^2 R_0^3} + \frac{1}{2}\frac{\delta^2}{\omega_b^2}(n-j)\left(n+\frac{j}{2}\right) + i\frac{2\nu}{\omega_b R_0^2}\frac{\delta}{\omega_b}(n-j) \tag{8}$$

$$\beta_2(n,j) = \frac{3k+1}{2} + (3k-1)\frac{S}{\rho\omega_b^2 R_0^3} + \frac{1}{2}\frac{\delta^2}{\omega_b^2}\left(n^2 - nj - j^2\right) + i\frac{2\nu}{\omega_b R_0^2}\frac{n\delta}{\omega_b} \tag{9}$$

The acoustic signature of cavitation noise is broadband and has been subjected to various theoretical and experimental investigations. It is noteworthy that practically all experimental results are reported as a power spectral density derived from a Fourier analysis of the data.[18] There appears to be no report in the literature of the fine details in frequency resolution that could be obtained from Bayesian analysis or the transient details that would emerge from wavelet analysis.

The conventional understanding of the character of the acoustic signature is as follows. The dominant frequency is related to the natural frequency of the typical cavitation bubble. This is related to the size of the nucleation site, but there are many nucleation sites and they have a distribution of sizes. There is a critical frequency, f, such that $ft_{TC} = 1$, where $t_{TC} = 0.915R_0[\rho_L/(p_\infty - p_v)]$ - is the collapse time of the bubble whose most probable nucleation radius is R_0. At the critical frequency, the power spectral density is highest. Well below the critical frequency, the power spectral density increases as f^4. Well above the critical frequency, the power spectral density decreases approximately as $1/f^2$. Different researchers have reported different results for the complex behavior near the critical frequency. [It would be of great interest to examine this region using Bayesian analysis.]

As cavitation becomes severe, the cavitation bubbles cannot be assumed to act independently of each other.[17] A cloud of interacting bubbles forms. This is a serious concern because the collapse of the bubble cloud causes considerably more damage than the collapse of an isolated bubble. The natural frequency of the bubble cloud is a fraction of the individual bubble.[19] Hence, it is expected that the frequency of AE should drop as cavitation becomes more severe. There is anecdotal evidence that this kind of behavior does occur.

It is noteworthy that in a bubbly liquid medium for natural frequencies above 200 kHz, the attenuation of the pressure wave is about 5 dB/cm, as compared to 25 dB/cm at the average bubble natural frequency of 100 kHz. Thus, even if the higher frequency effects may occur less commonly, they may still be as easy to observe as the low frequency events that start out stronger. Another way to interpret this is to note that although most of the energy is generated near the average bubble natural frequency, these bubbles act as absorbers. Energy from the collapse of bubbles far away from the average size is smaller, but since it is not so strongly absorbed, it may be easier to detect.[20]

In a bubbly flow, there is a shock wave. Viscosity will affect the properties of the shock wave and lead to damping effects. For reasonably low void fractions, the shock wave ringing effect occurs at about half the natural frequency of the isolated bubble. In the time domain, at a stationary observation point, the shock wave will be perceived as a rising and then damped nonlinear oscillation. The shock wave contributes to the acoustic signature in cavitating flows. Equation 9 may be particularly relevant to the Bayesian analysis suggested for subsequent research.[21]

$$\begin{aligned}&\left(1-\alpha_1+\alpha_1 r^3\right)^2 r\frac{d^2r}{dz^2}+\frac{3}{2}\left(1-\alpha_1+\alpha_1 r^3\right)\left(1-\alpha_1+3\alpha_1 r^3\right)\left(\frac{dr}{dz}\right)^2\\&+\left(1-\alpha_1+\alpha_1 r^3\right)\frac{4\nu_L}{u_1 R_1}\frac{1}{r}\frac{dr}{dz}+\alpha_1(1-\alpha_1)\left(1-r^3\right)\\&=\frac{1}{u_1^2}\left[\frac{(p_1-pv)}{\rho_L}\left(r^{-3k}-1\right)+\frac{2S}{\rho_L R_1}\left(r^{-3k}-r^{-1}\right)\right]\end{aligned} \tag{10}$$

The situation likely to be encountered is the oscillating, flowing bubble cloud. This will have a number of modes and a number of natural frequencies, all lower than the natural frequency of an isolated bubble. For a small void fraction, all the cloud natural frequencies will be in a narrow range just below the isolated bubble natural frequency. For a large void fraction, the cloud natural frequencies will occupy a large range below the bubble natural frequency. Since damping is strong near the isolated bubble natural frequency and since the outside of the cloud shields the rest of the world from effects inside the cloud, the dominant effect in a cloud in a damping medium is the response at the lowest cloud natural frequency. Thus, the response will be seen as a large peak at the lowest cloud natural frequency and a smaller peak at the bubble natural frequency, with the strength and frequency of the cloud response decreasing with increasing void fraction.[19]

Note that the foregoing paragraph only describes the linear effects of a bubble cloud in a flow. Other effects at higher frequencies occur when nonlinear effects are taken into account. Harmonic cascading is the effect of harmonics at relatively low frequencies exciting the natural frequencies of smaller bubbles, leading to higher frequency effects. Whereas the linearized analysis of bubble cloud dynamics showed the lowest cloud natural frequency as the dominant effect, nonlinear analysis says that the low-order harmonics of the lowest cloud natural frequency are also strongly present. This can stimulate harmonic cascading if the fluid contains nucleation sites over a range of small sizes. Fine resolution at high frequencies is needed to observe harmonic cascading. Previous researchers typically used Fourier analysis at 1/3-octave resolution to analyze experimental data.[17] Bayesian methods should dramatically reveal harmonic cascading. In addition, if the bubbles are not spherical, super-resonant effects can occur.[22]

Note that the isolated bubble natural frequency is the key to understanding the expected acoustic effects of a cavitating flow. The distribution of sizes of nucleation sites will cause AE to be spread out about the natural frequency of the average nucleation radius. The shock wave will produce a strong signature in the region 0.1-0.9 of the isolated bubble natural frequency. The cloud effects will produce more energy just below the natural frequency.[17]

If the strength of excitation is such that the weakly nonlinear solution applies, then the response will be one of the following conditions. The response is *subresonant* if the excitation is at a frequency lower than the lowest natural frequency of the bubble cloud. The response is *transresonant* if the excitation is at a frequency higher than the lowest natural frequency of the bubble cloud but lower than the natural frequency of the average bubble in the cloud. The response is *super-resonant* if the excitation is at a frequency higher than the natural frequency of the average bubble in the cloud. Super-resonance response decays fairly rapidly with distance from the source of excitation. It is strongest in the center of the cloud and weakens toward the edges.[17]

The harmonic cascade is predicted by Kumar.[17] Harmonic cascades should be a common occurrence in practical experiments. High-resolution frequency spectra should reveal them.[23]

Model-based Analysis

Anticipatory Systems

Where conventional condition monitoring analysis falls short is where an anticipatory system can provide something genuinely valuable due to the fact that it can detect an incipient catastrophe.[4] It emulates the mechanism by which living creatures anticipate and avoid catastrophic dangers. An anticipatory system contains a model of itself, its environment, and adaptive models that emulate the associative (learned) behaviors of a biological system. These models operate faster than real-time, providing a prediction about the near future, which the anticipatory system can use to change its own behavior to avert the catastrophe. The internal models in an anticipatory system may appear to be quite simple, but still be able to capture catastrophic behavior.

Bayesian Parameter Estimation

The most effective available method for identifying a model from experimental data is Bayesian parameter estimation.[24] In addition to extracting the model parameters from the data, it gives a measure of the goodness of the estimate. Most importantly for this type of application, Bayesian provides the optimal method for extracting a signature from data when the signature is obscured by other effects. Thus, Bayesian parameter estimation provides a practical means of determining the models for an anticipatory system from observed data.

Modeling the Onset of Cavitation

Amazingly there are many things that can go wrong with a pump and each of these can be modeled. However, a complete model of a pump is far beyond the scope of this project. Therefore, we investigated a single effect—cavitation.

There are several reasons for this choice. First, cavitation is a widely occurring undesirable operating condition. It occurs abruptly and its onset is not predictable by conventional methods. In addition, to keep cavitation from occurring, pumps are operating conservatively far from the point at which cavitation might start. Nevertheless,

cavitation is easily controlled by manipulating the pump input and output pressures. With a reliable signal warning of its onset, a cavitation control system could enable a pump to avoid cavitation completely, even if the pump operates very near the point of its onset.

This cannot be effectively done by conventional methods because while pumps do not wear out, they do wear. As a consequence of wear and other evolving effects, one of the pump properties that changes over time is the point at which a catastrophic effect such as cavitation begins to occur. Thus, it is not practical to make a one-time or occasional observation of the point of onset of cavitation and then assume it will remain fixed. A feature (descriptor) must be observed that indicates that cavitation is about to occur.

Although cavitation is a catastrophic effect, the physics of cavitation is reasonably well understood. A nonlinear model of fluid dynamics that includes extractable parameters of the acoustic signature and describes the onset of cavitation is readily constructable without basic research. Thus, cavitation is an ideal effect for demonstrating the utility of CD-CBM anticipatory systems. Since it is catastrophic, it is not reliably predictable by conventional methods. Since it is well understood, an anticipation model can be formulated from experimental data and the existing physics.

Proof-of-Concept: Experiment and Analysis

The proof-of-concept CD-CBM System (anticipatory model) was developed and applied to a chamber on a flow loop at Oak Ridge National Laboratory (ORNL). The flow loop (shown in Figure 1) which is used in this test and standard calibration studies at ORNL is NIST qualified. To eliminate risk and any damage to the system, a venturi spool piece was fabricated and inserted into the loop. Figures 2 and 3 are the spool piece and test flow loop, respectively. Wide and narrowband ultrasonic probes were used to acquire the high frequency phenomena. Figure 4 shows the ultrasonic probes on the venturi tube mounts.

The venturi chamber was designed specifically for this experiment. It was instrumented with conventional flow, temperature and pressure sensors and several channels of AE sensors with frequency responses up to approximately 400 kHz (1 MHz). The objective was to show that precursors of cavitation and signatures of incipient and severe cavitation could be detected and made available to an anticipatory system.

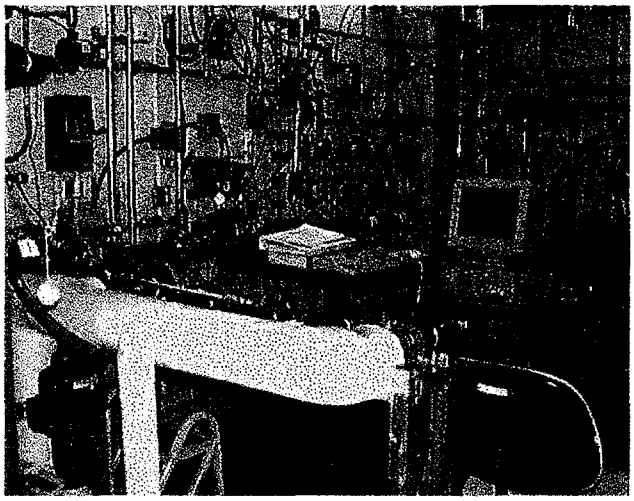

Figure 1. ORNL standard flow loop used in cavitation studies.

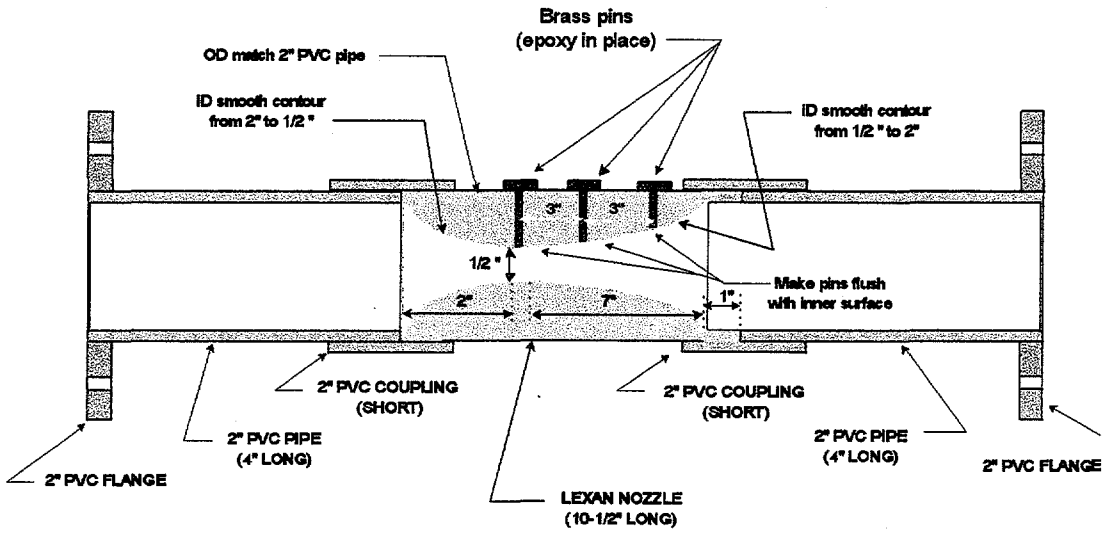

Figure 2. Venturi spool piece design used to affect cavitation in the ORNL flow loop.

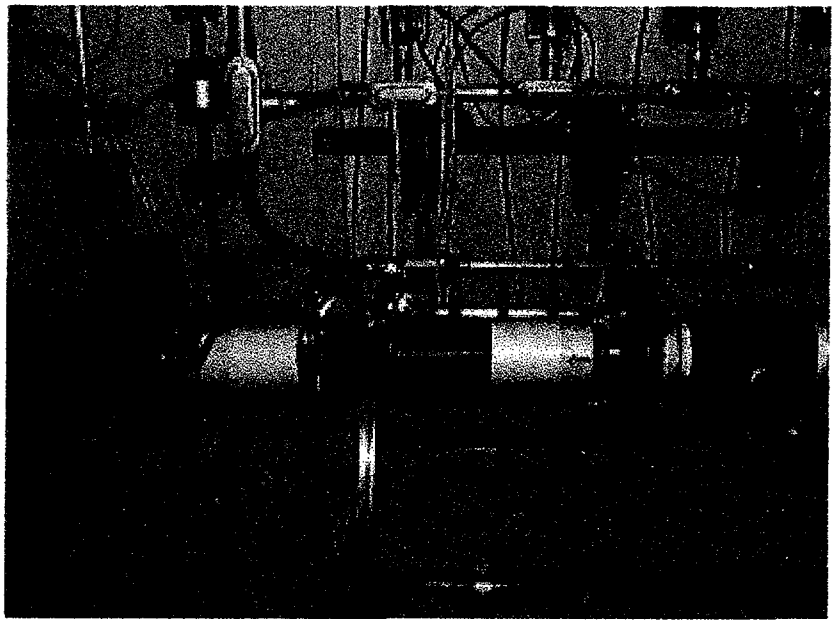

Figure 3. Venturi spool piece inserted into ORNL flow loop.

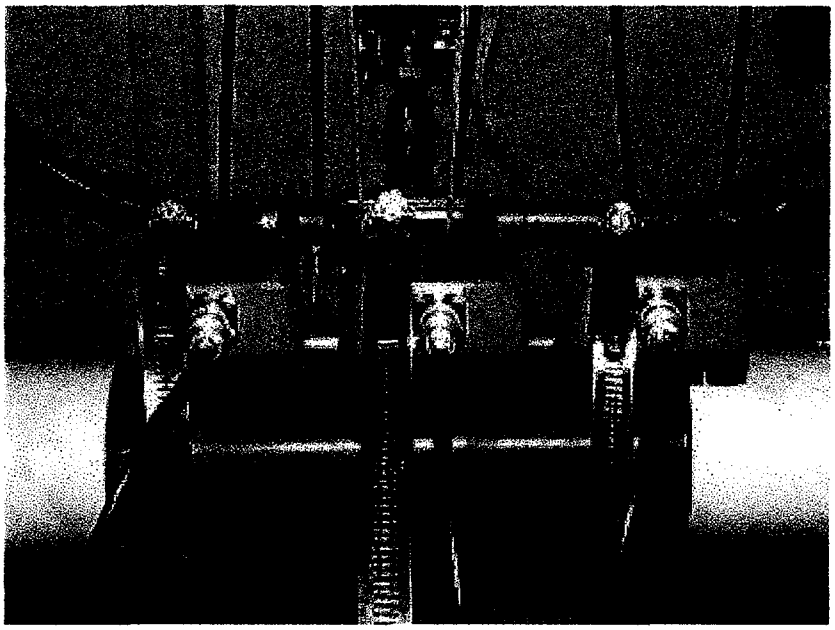

Figure 4. Ultrasonic probes on venturi tube mounts.

Preliminary Systems Analysis and Operational Survey

A survey of conventional practices on pump maintenance led to the conclusion that there are many failure modes and operational issues related to pump problems. Understanding them all is well beyond the scope of Phase I. With this in mind, it was decided to limit the investigation to cavitation in general.

Cavitation was selected for several reasons. It is a problem of widespread interest since it affects any device that comes in contact with fluids, including pumps. Cavitation is itself an undesired operating mode for pumps. But operating a pump at the point just below incipient cavitation is not. It is highly desirable and efficient to operate a pump at this state—especially if the point of incipient cavitation is anticipated. In addition, cavitation damage is a direct cause of catastrophic failure of fluid handling devices. If cavitation is deliberately allowed to occur (perhaps because an operational contingency requires it), but its severity and duration are accurately monitored, it should be practical to predict cavitation damage and take the cavitating device out of service just before it fails. The accurate determination of the remaining life of an element that is event driven is a critical operating parameter.

Furthermore, it appears that previously unsolved problems in cavitation monitoring appear to be tractable by newly emerging methods. For example, previous researchers suspected that there were usable cavitation features in AE above 100 kHz but lacked the hardware to investigate them.[24] The investigation with a high bandwidth, wide dynamic range instrument shows the AE spectrum in the 100-500 kHz region to be rich in cavitation features. Modeling these features with Bayesian parameter estimation is tractable. Using the resulting models in a CD-CBM anticipatory system should lead to a practical anticipation engine for cavitation.

Define and Develop Process Feature Vectors for Pumps

The project has focused on cavitation. In order to take the most direct possible look at cavitation features, the experiment was designed to minimize all others. The idea is that once the cavitation and precursor features are known, it would be straightforward to describe them with a Bayesian model and to use this model to extract these same features from noisy and cluttered signals. Based on this strategy, a venturi chamber was used instead of a pump. This experimental approach was designed to produce cavitation in a controlled manner while minimizing other effects.

As stated earlier, the flow loop was instrumented with conventional temperature, flow and pressure measuring devices, and AE sensors. The flow rate through the venturi chamber was precisely controlled at various fixed rates and the resulting signatures were collected. The conditions ranged from no flow to severe cavitation. AE signatures and correlated parameter data were collected for all these conditions. The results of this study are reported in the **Preliminary Experimental Analysis** section.

To obtain cavitation signature data, the cavitation nozzle (see Figure 2) was inserted in the flow loop. Three brass pins were embedded in the body of the nozzle to provide a low loss propagation path for AE features being generated. The three pins provided a look at three different throat diameters of the nozzle. The head of the pin provided a convenient surface for abutting the sensitive surface of the AE sensor element.

Develop and Deploy a Baseline Proof-of-Concept Context-dependent Monitoring System

The proof-of-concept consisted in showing the distinguishing features of impending, incipient, and severe cavitation are present in AE of each of these types of flows. These features were observed in the venturi chamber in the flow loop described above and are typically decaying oscillatory bursts with a downward chirp in frequency. The observed signatures are consistent with the "harmonic cascade" theory of incipient cavitation. The formal structure of the feature vector developed as a result of this study is:

$$fv \Rightarrow [\langle e^{-\gamma t}\cos(\omega t\kappa+\alpha\kappa^2t^2),\ e^{-\gamma t}\sin(\omega t\kappa+\alpha\kappa^2t^2),\{\omega=a,\ \gamma=b,\ \alpha=c\},\ cf=[0,1]]. \quad (11)$$

The context-dependent monitoring device was a Vallen Systeme AMSY4-MC6 AE Monitor (Vallen ID number 40900). A complete set of AE signatures at various flow rates was collected with broadband piezo-electric AE sensors (Vallen SE-1025-H, usable frequency response from 10 kHz through greater than 400 kHz). Another complete set of AE signatures at various flow rates was collected with broadband piezo-electric AE sensors (Vallen SE-9125-M, usable frequency response from 20 kHz through 200 kHz). In order to capture hysteresis effects in both cases, the data were collected by incrementing the flow rate both upward and downward. The context was monitored with conventional flow loop sensors whose outputs were converted to voltages and recorded by the parametric input channels of the Vallen AE Monitor.

Experimental Data: Broadband Sensors

One set of data was collected with a broadband AE sensor (10-400 kHz - Channel 1) connected to the middle pin of the cavitation nozzle and another broadband AE sensor (Channel 2) connected to the pin at the wide end of the cavitation nozzle. Figures 5 through 46 show the evolution of the AE signature as the flow rate increases from zero to severe cavitation and then back to zero.

Figure 5 shows typical signatures from the two sensors when they are in a padded box and sensing essentially no AE energy from the environment. The noise generated by the sensor and their associated electronics is shown. The plots are consistent with the manufacturer's claim that the noise floor of the AE system is approximately 1 μV. The left-hand plots are the time-domain data and inside each time domain plot is a time window. The right hand plots are the discrete Fourier transform (DFT) of the data inside the time window.

Figure 6 shows the signatures from Channel 2 at two different times at a flow rate of 5 gallons per minute (gpm). It appears indistinguishable from the electronic noise.

Similar signatures were collected on both channels at flow rates between 5 and 11 gpm and are indistinguishable from the electronic noise of the sensor. At a flow rate of 12 gpm, the first features begin to appear that may be more than noise. One such rare instance is shown in Figure 7. These data should be analyzed with Bayesian parameter estimation to determine if this is a deterministic signature or merely wishful thinking.

In the course of this experiment, three distinct types of AE patterns were captured and two of these types were observed at a flow rate of 13 gpm with the broadband sensors, as shown in Figure 8. A decaying "chirp-down" pulse was captured in Channel 1 as seen in the top frame. A signal similar in appearance to a chaotic time series (but perhaps only noise) is shown in the middle frames. A signal that looks a bit like a modulated carrier is shown in the bottom frame.

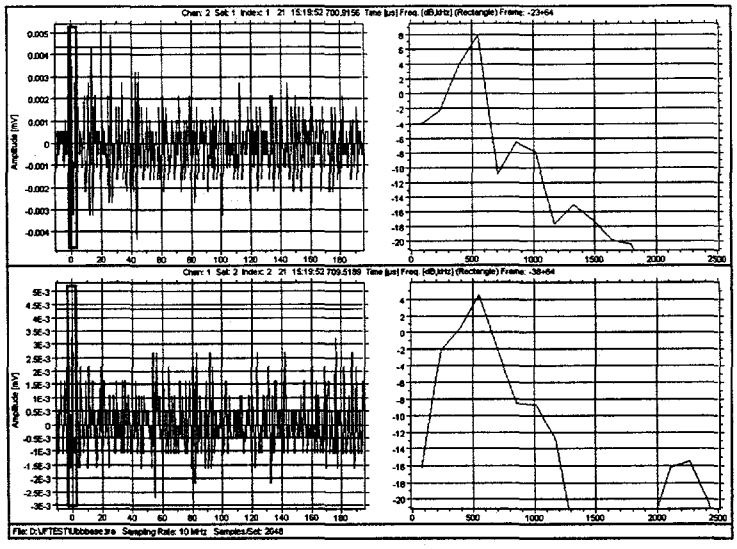

Figure 5. Noise from broadband sensors.

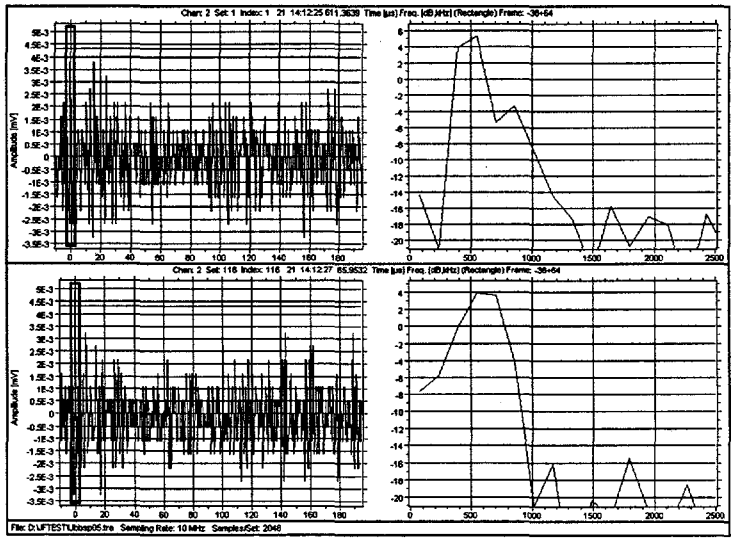

Figure 6. Broadband sensors flow rate: 5 gpm.

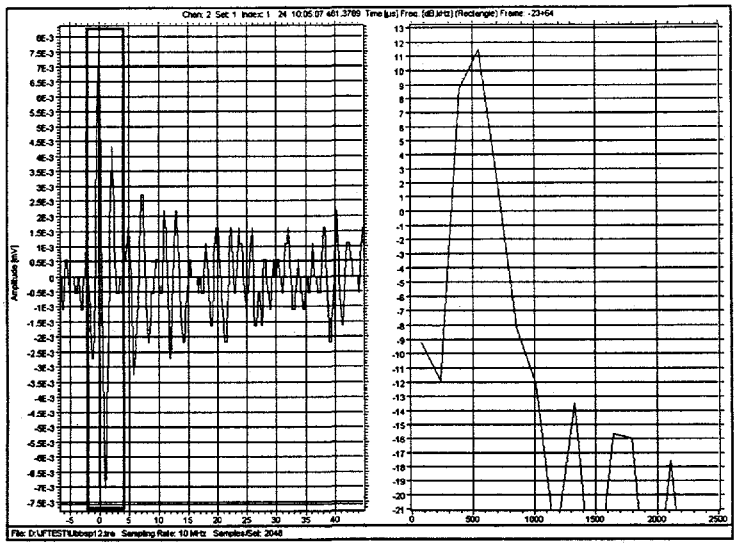

Figure 7. Broadband sensors flow rate: 12 gpm.

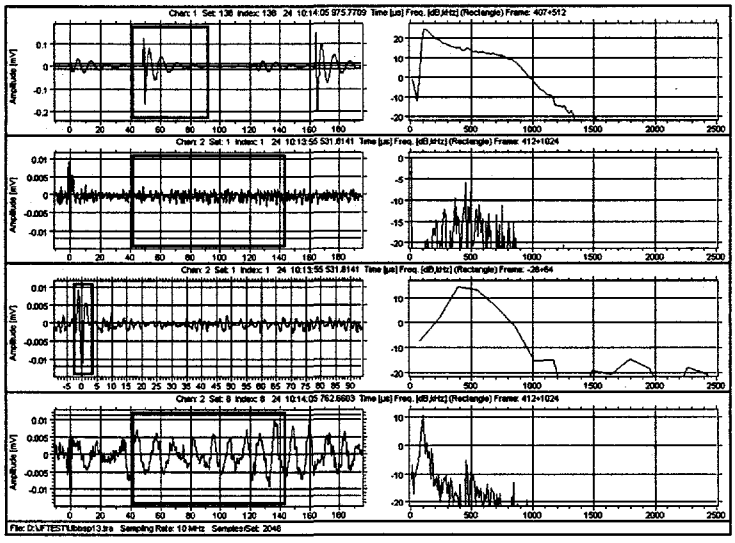

Figure 8. Broadband sensors flow rate: 13 gpm.

As shown in Figure 9, the signatures at 14 gpm do not appear to differ substantially from electronic noise.

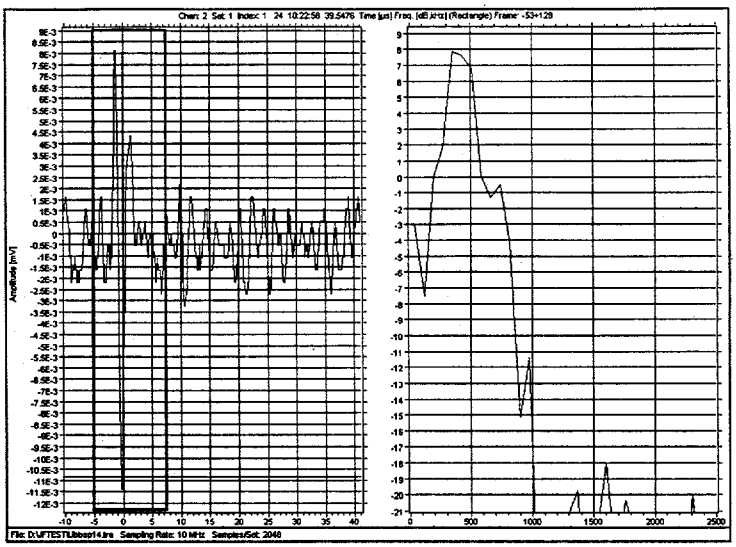

Figure 9. Broadband sensors flow rate: 14 gpm.

At a flow rate of 15 and 16 gpm, cavitation precursor features may be beginning to appear. In the time window in the bottom frame of Figure 10 is a burst that may be a genuine signal. Another such burst appears in the time window in the top frame of Figure 11. These data should be analyzed with Bayesian parameter estimation to determine if these are deterministic signatures.

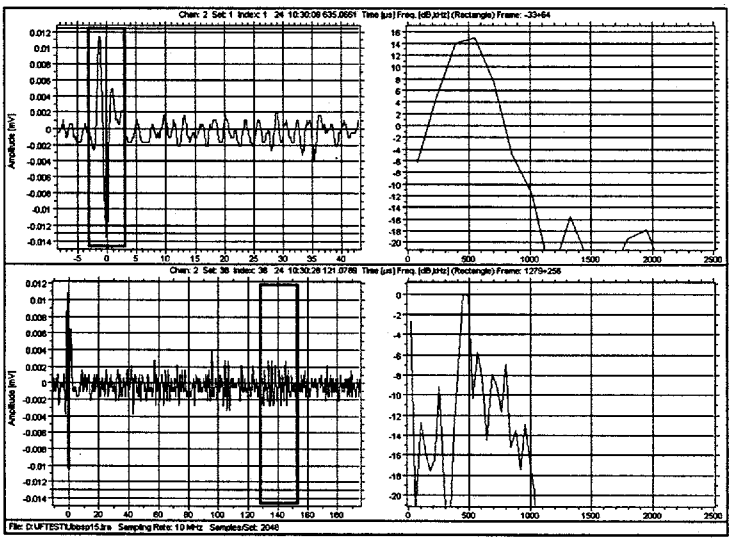

Figure 10. Broadband sensors flow rate: 15 gpm.

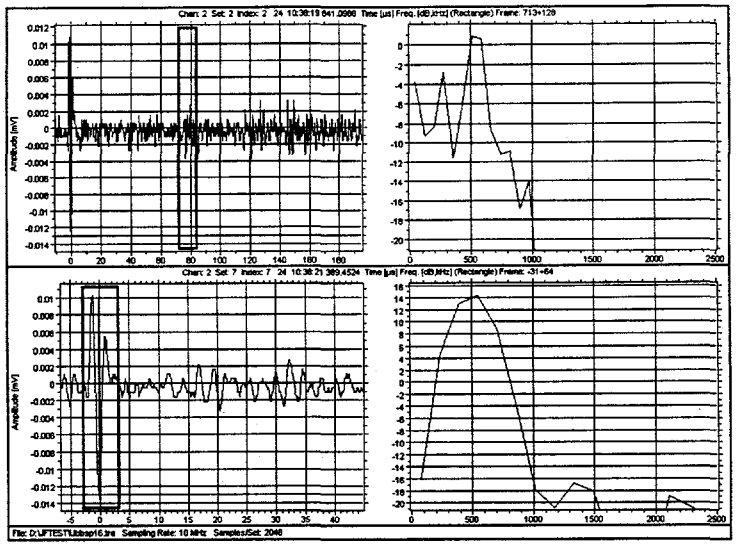

Figure 11. Broadband sensors flow rate: 16 gpm.

At a flow rate of 17 gpm, unmistakable features are beginning to appear. In the time windows in the top three frames of Figure 12 are several deterministic bursts. Are these cavitation precursors?

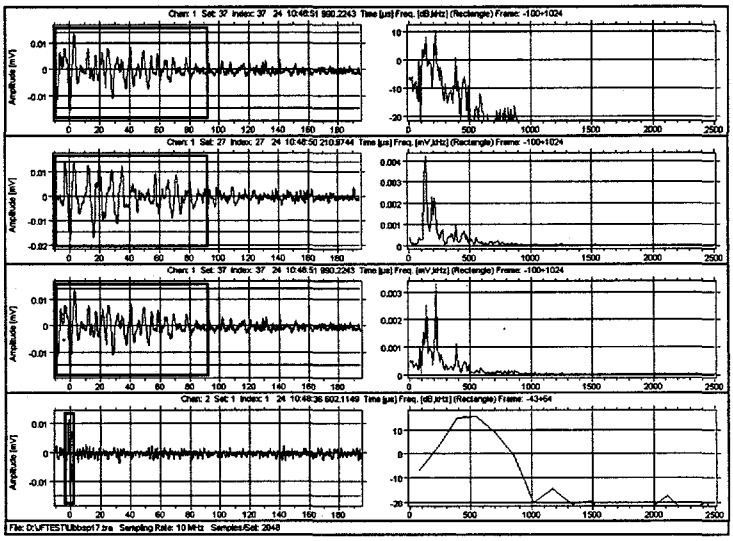

Figure 12. Broadband sensors flow rate: 17 gpm.

At a flow rate of 18 gpm, as shown typically in Figure 13, all captured events looked like electronic noise. Are there cavitation precursors buried in the noise?

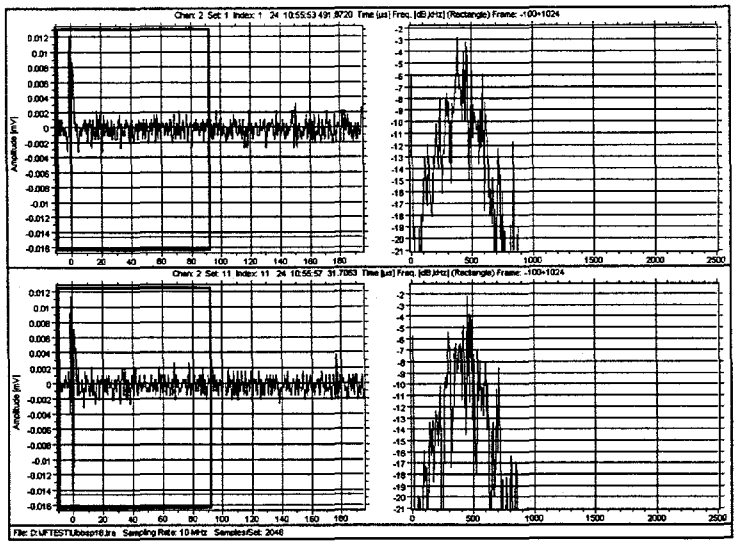

Figure 13. Broadband sensors flow rate: 18 gpm.

At a flow rate of 19 gpm, most captured events looked like electronic noise. All the exceptions are shown in Figure 14. In both channels, signals that appear similar to chaotic time signatures are captured. The bottom frame shows a modulated signal. The top frame shows electronic noise that may, or may not, have some weak embedded signatures.

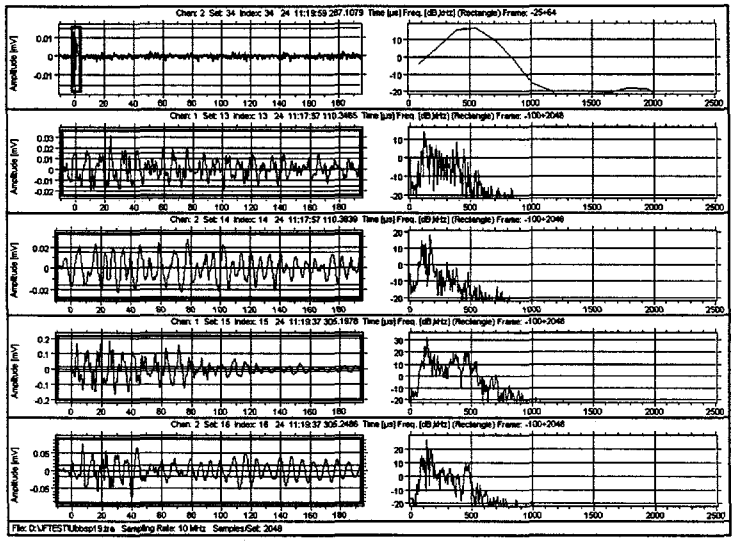

Figure 14. Broadband sensors flow rate: 19 gpm.

At a flow rate of 20 gpm, most captured events looked like electronic noise. The sole exception is shown in Figure 15. The bottom frame shows a modulated signature. At 20 gpm, the cavitation nozzle was beginning to crackle audibly.

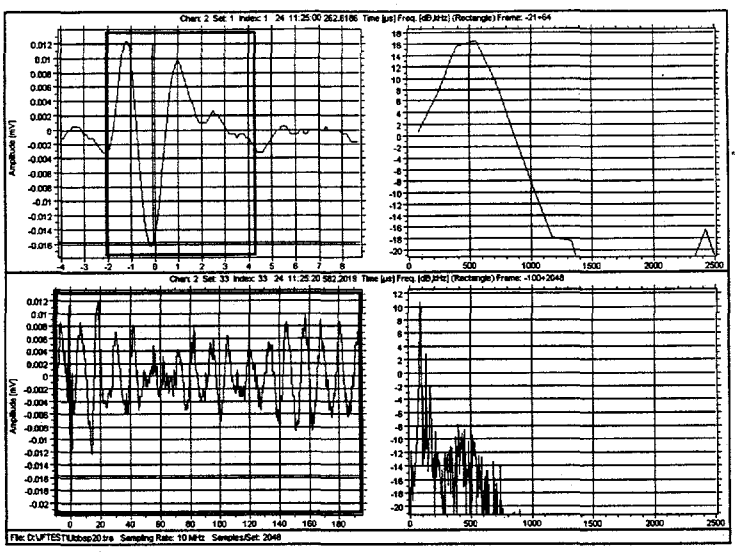

Figure 15. Broadband sensors flow rate: 20 gpm.

At a flow rate of 25 gpm, all captured events were decaying "chirp down" signals. As shown in Figure 16, these are captured in both channels. At 25 gpm, the cavitation nozzle was crackling very loudly.

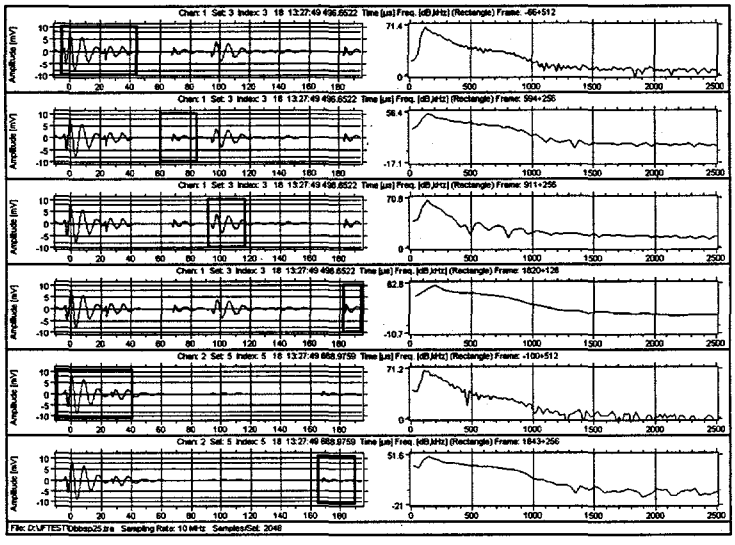

Figure 16. Broadband sensors flow rate: 25 gpm.

The preceding data were captured by starting at zero-flow and incrementing the flow rate upward. In order to observe a suspected hysteresis effect, the following data were captured by decrementing the flow rate from 25 gpm. All captured events were decaying "chirp down" signals at 24 gpm, but were slightly weaker than those captured at 25 gpm. As shown in Figure 17, these are captured in both channels.

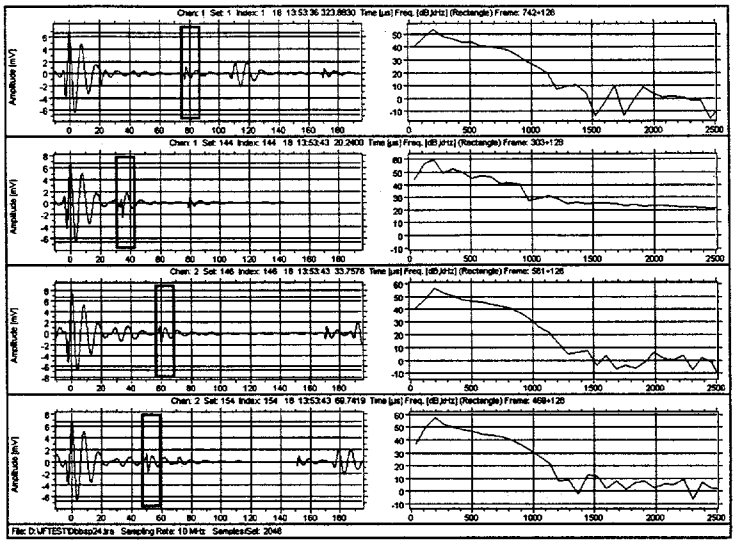

Figure 17. Broadband sensors flow rate: 24 gpm.

At 23 gpm all captured events were decaying "chirp down" signals but were slightly weaker than those captured at 24 gpm. As shown in Figure 18, these are captured in both channels.

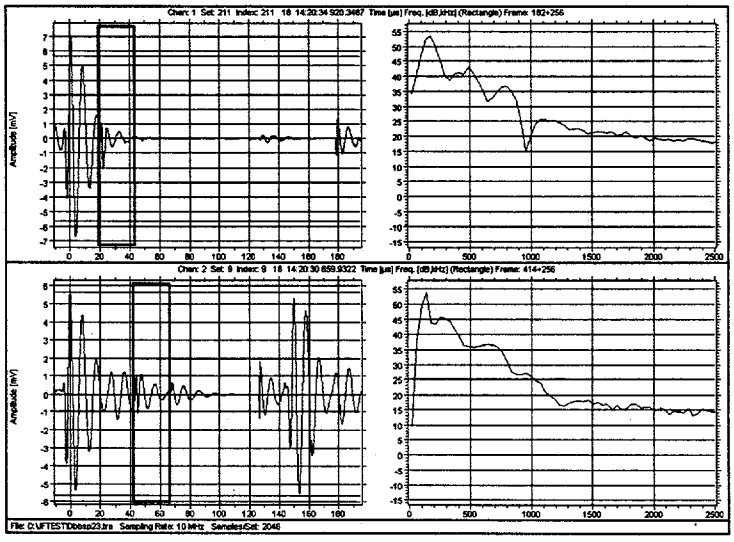

Figure 18. Broadband sensors flow rate: 23 gpm.

At 22 gpm all captured events were decaying "chirp down" signals but were slightly weaker than those captured at 23 gpm. As shown in Figure 19, these are captured in both channels.

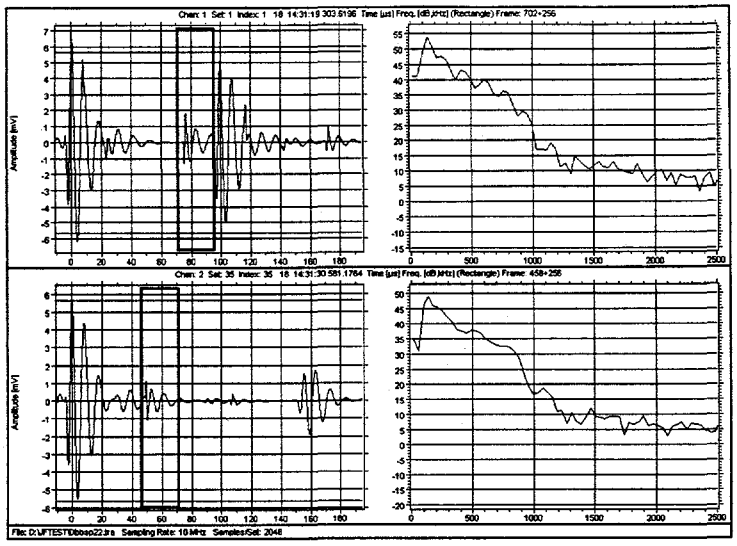

Figure 19. Broadband sensors flow rate: 22 gpm.

At 21 gpm all captured events were decaying "chirp down" signals but were slightly weaker than those captured at 22 gpm. As shown in Figure 20, these are captured in both channels.

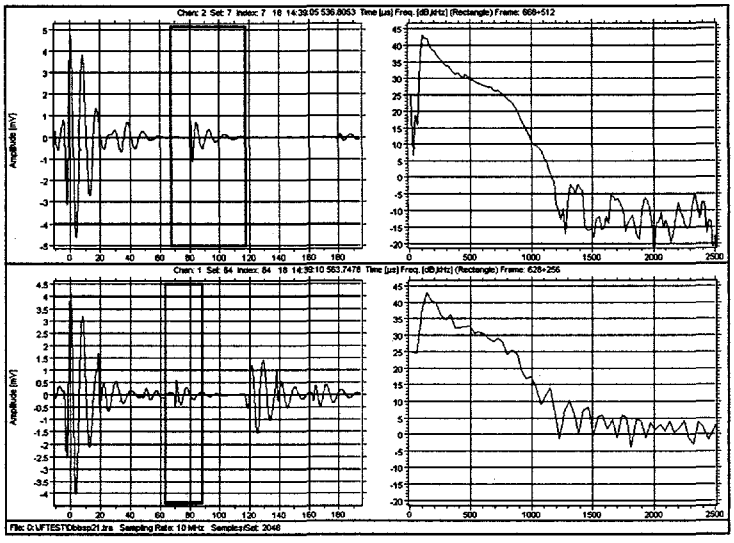

Figure 20. Broadband sensors flow rate: 21 gpm.

At 20 gpm all captured events were decaying "chirp down" signals but were slightly weaker than those captured at 21 gpm. As shown in Figure 21, these are captured in both channels. However, these events are rare in Channel 2 (where cavitation nozzle is wide) and common in Channel 1 (where cavitation nozzle is narrow).

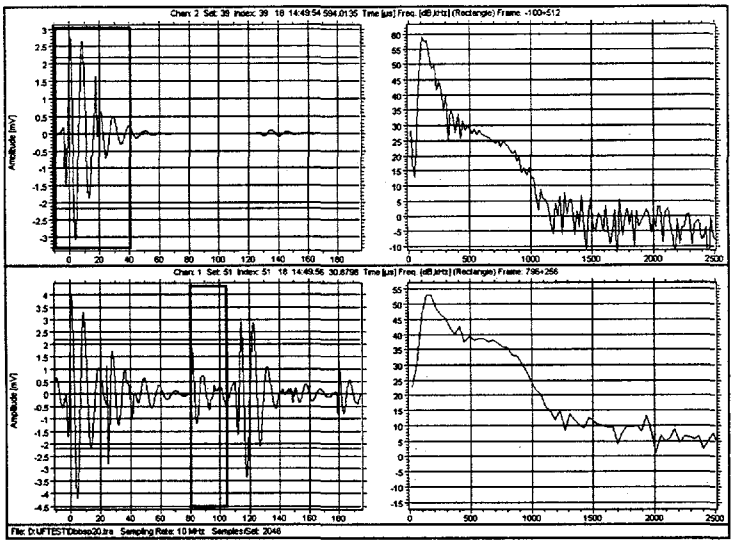

Figure 21. Broadband sensors flow rate: 20 gpm.

At 19 gpm most captured events were decaying "chirp down" signals but were slightly weaker than those captured at 20 gpm. Some "chaotic" events were observed. As shown in Figure 22, these are captured in both channels. Note that as the flow rate is decremented, the chirps are occurring at lower flow rates than when the flow rate was being incremented. This is the hysteresis effect.

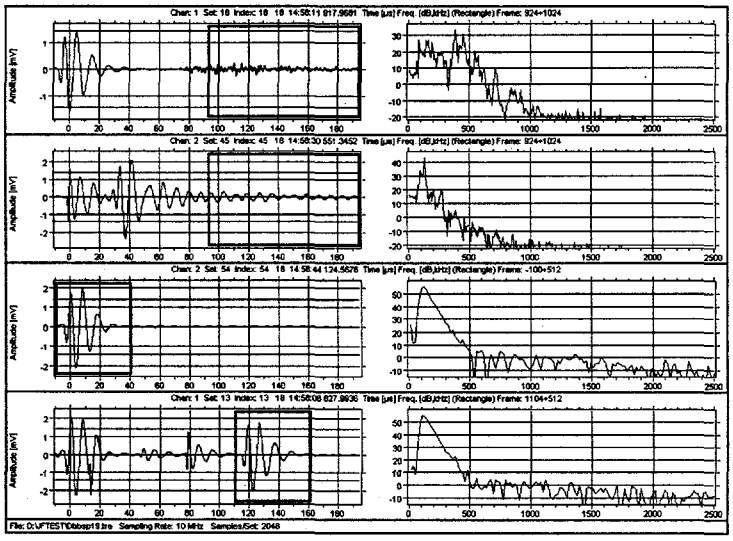

Figure 22. Broadband sensors flow rate: 19 gpm.

At 18 gpm most captured events were decaying "chirp down" signals but were slightly weaker than those captured at 19 gpm. One "chaotic" event was observed. As shown in Figure 23, this was captured in Channel 1, the narrower

throat radius. Note that as the flow rate is decremented, the chirps are still occurring at lower flow rates than when the flow rate was being incremented. This is the hysteresis effect.

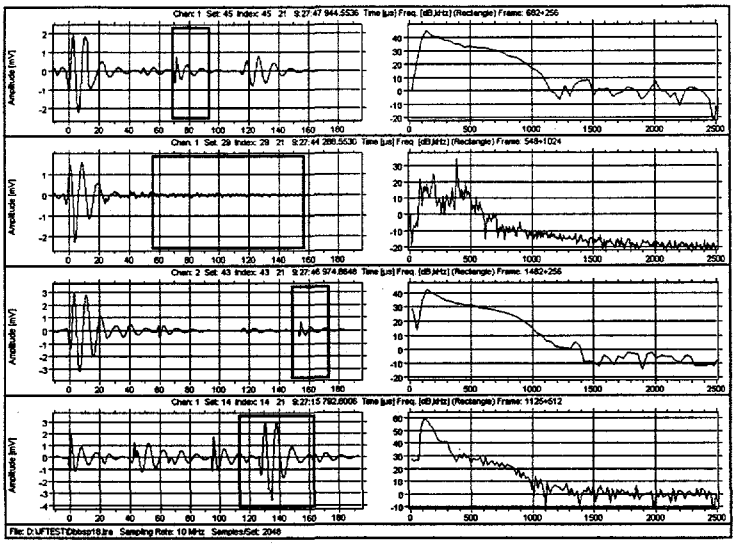

Figure 23. Broadband sensors flow rate: 18 gpm.

At 17 gpm no captured events were decaying "chirp down" signals. The "downward" threshold of cavitation appears to be between 17 and 18 gpm. Note that as the flow is decremented from 18 to 17 gpm, the sensor output abruptly drops from millivolts to microvolts, which is strongly suggestive of a state change. Figure 24 may contain some cavitation precursors buried in the noise. This should be investigated with Bayesian parameter estimation.

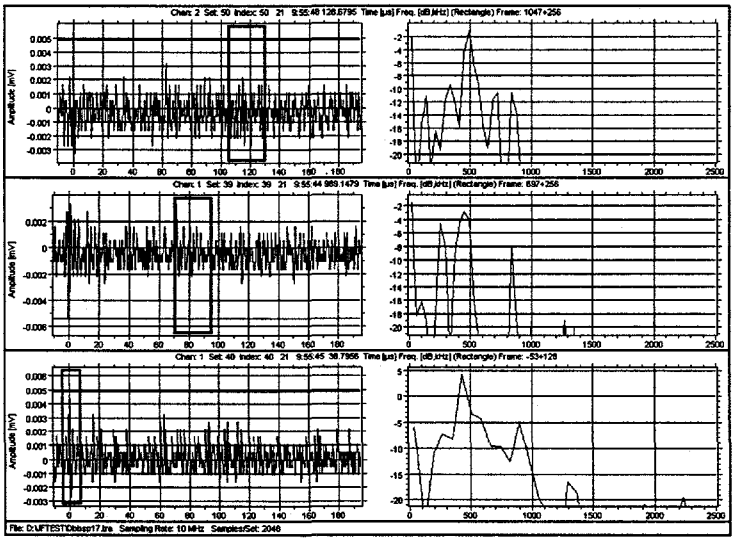

Figure 24. Broadband sensors flow rate: 17 gpm.

At 16 through 12 gpm no captured events contained obvious deterministic elements. There were a few events in both channels that may have been weak signals buried in noise. The signals shown in the time windows in Figure 25 at a

flow rate of 12 gpm are typical. These should be investigated with Bayesian parameter estimation to determine if they contain any useful features. No decremented data were captured from 11-5 gpm.

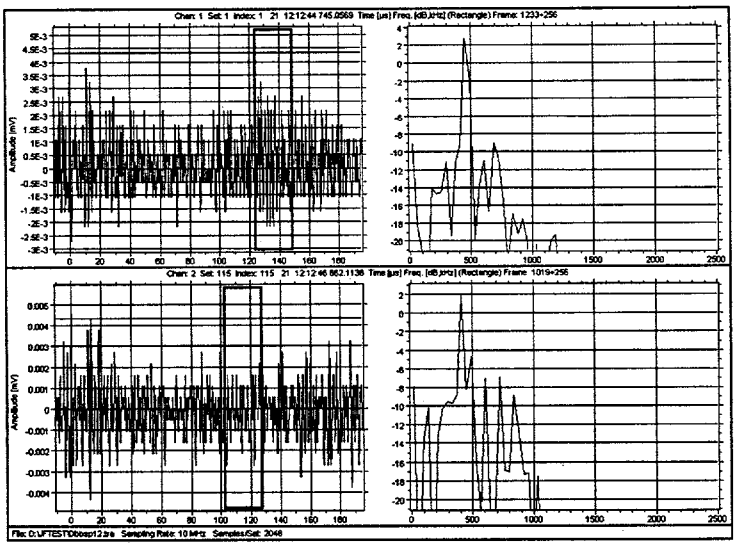

Figure 25. Broadband sensors flow rate: 12 gpm.

Wishful thinking can be deceptive. After the 12 gpm data were taken, the flow in the flow loop was completely shut off. As shown in the time windows in Figure 26, the sensor output still contains elements that appear to the eye as weak deterministic signals.

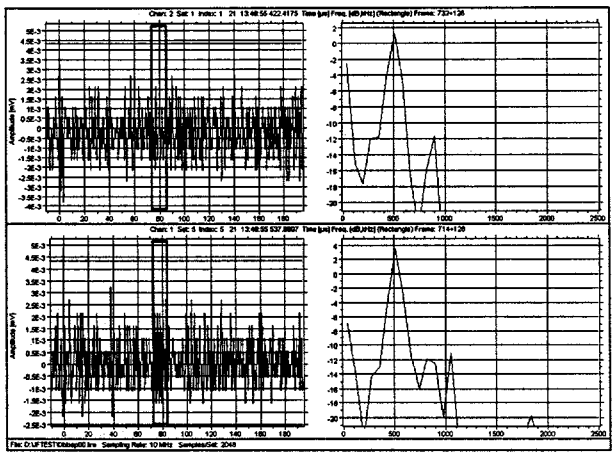

Figure 26. Broadband sensors flow rate: 0 gpm.

Experimental Data: Narrowband Sensors

Another set of data was collected with a narrowband AE sensor (25-175 kHz - Channel 2) connected to the middle pin of the cavitation nozzle; another set with a narrowband AE sensor (Channel 1) connected to the pin at the wide end of the cavitation nozzle; and another narrowband AE sensor (Channel 3) connected to the pin at the narrow end of the cavitation nozzle. The following figures show the evolution of the AE signature as the flow rate increases from zero to severe cavitation and then back to zero.

Figure 27 shows typical signatures from the three sensors when they are mounted on the flow loop with zero flow. The noise generated by the sensor, its associated electronics, and the environment is shown. The plots are consistent with the manufacturer's claim that the noise floor of the AE system is approximately 1 μV. The left-hand plots are the time-domain data and inside each time domain plot is a time window. The right-hand plots are the DFT of the data inside the time window.

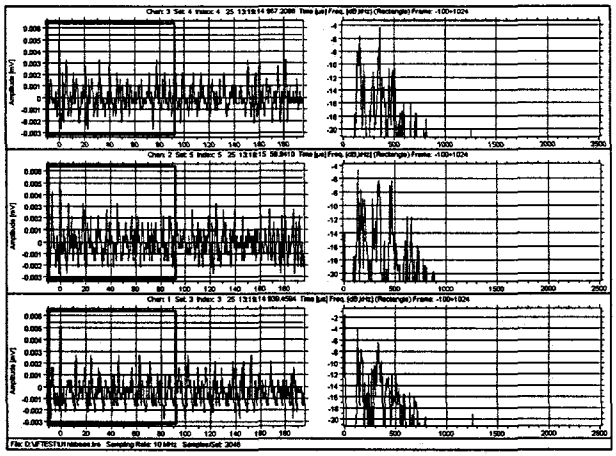

Figure 27. Noise from narrowband sensors.

At a flow rate of 12 gpm, the first features may be beginning to appear in the noise. One such instance is shown in Figure 28. These data should be analyzed with Bayesian parameter estimation to determine if this is a deterministic signature or merely wishful thinking.

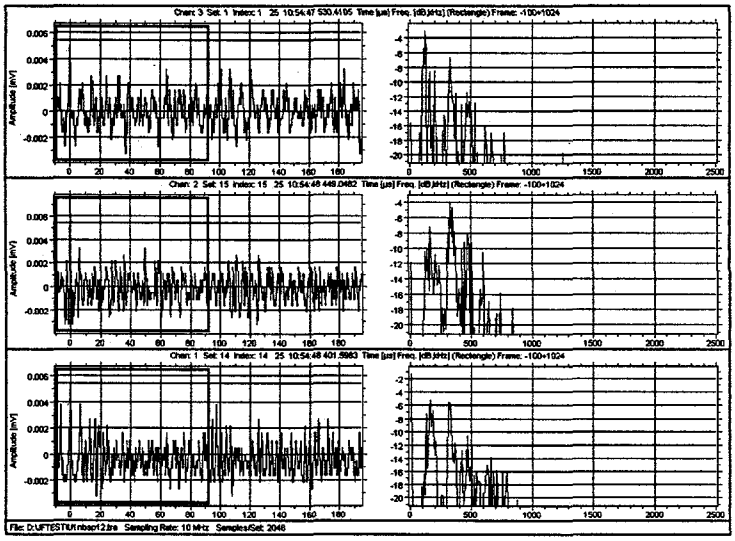

Figure 28. Narrowband sensors flow rate: 12 gpm.

At a flow rate of 13 gpm with the narrowband sensors, as shown in Figure 8, somewhat stronger features than those at 12 gpm may be appearing in the noise. One such instance is shown in Figure 29. These data should be analyzed with Bayesian parameter estimation to determine if this is a deterministic signature or merely even more wishful thinking.

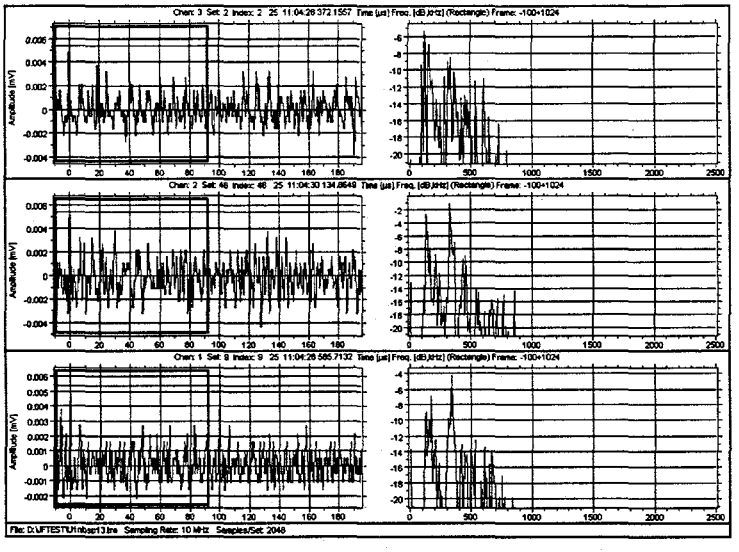

Figure 29. Narrowband sensors flow rate: 13 gpm.

As shown in Figure 30 the signatures at 14 gpm do not appear to differ substantially from electronic noise in Channel 1 where the throat is widest, but may show modulation in Channel 2 and quite a distinct signature in Channel 3, where the throat is narrowest. This is consistent with the expectation that where the throat is narrow, the velocity must be high and the pressure low. The lower the pressure, the more likely occurrence of cavitation features or precursors.

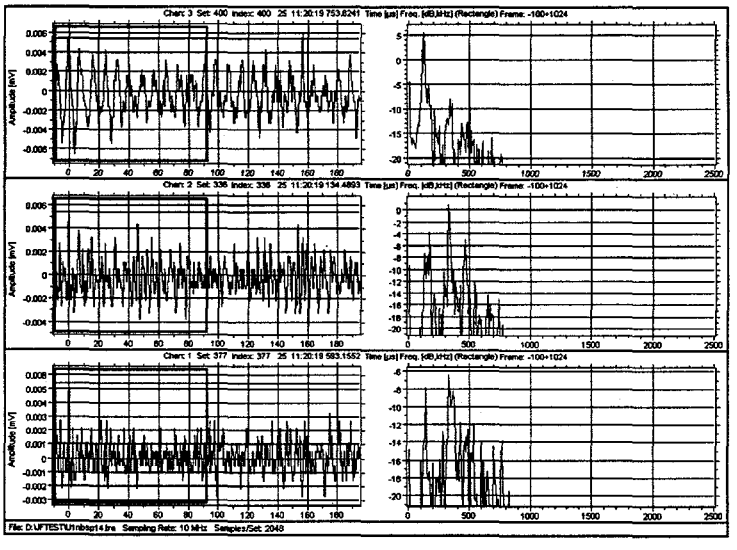

Figure 30. Narrowband sensors flow rate: 14 gpm.

At a flow rate of 15 and 16 gpm, strong deterministic features are clearly evident in Figures 31 and 32. Consistently nonrandom features appear at lower flow rates with the narrowband sensors than with the broadband sensors. This is not too surprising as the data taken with broadband sensors suggests that the dominant cavitation energy is in the vicinity of 100-150 kHz and the narrowband sensors favor this band. Thus providing a more favorable signal to noise ratio for the kinds of signals that may be cavitation signatures or precursors. Also for the narrowband data,

there is a sensor (Channel 3) mounted on the pin nearest the narrow part of the throat where cavitation is most likely to occur.

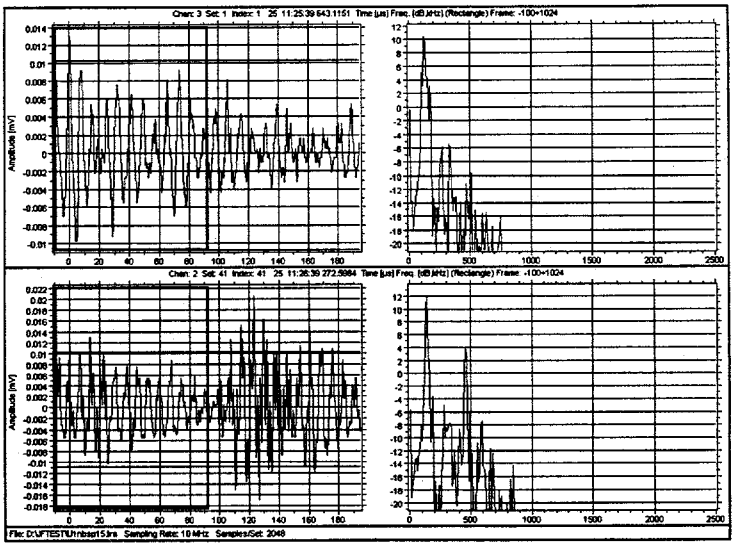

Figure 31. Narrowband sensors flow rate: 15 gpm.

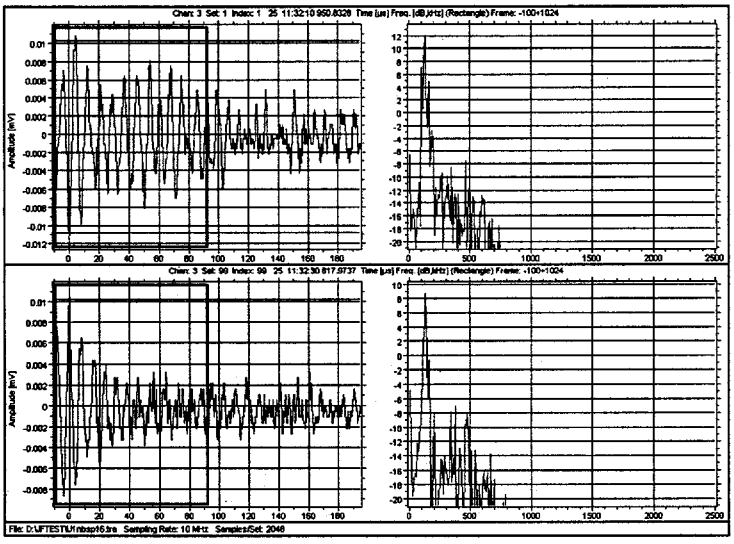

Figure 32. Narrowband sensors flow rate: 16 gpm.

At a flow rate of 17 gpm, a dominant broadband feature just above 100 kHz appears. This is shown in Figure 33.

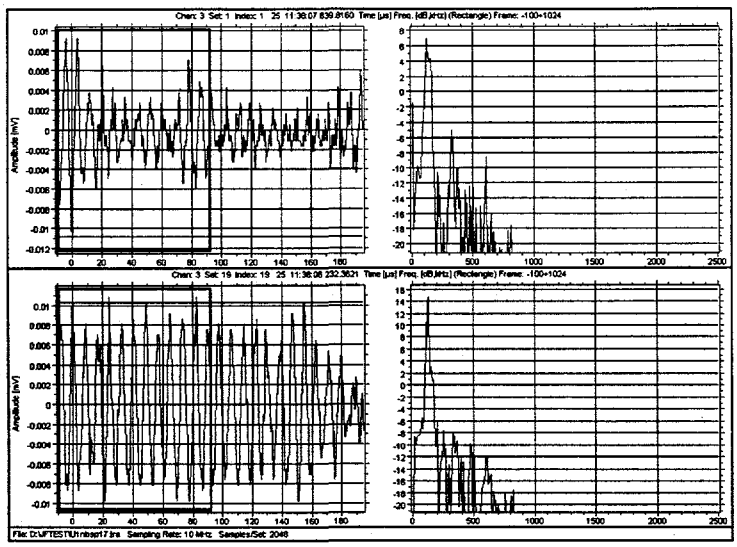

Figure 33. Narrowband sensors flow rate: 17 gpm.

At a flow rate of 18 gpm as shown typically in Figure 34, the events are similar to those at the 17 gpm flow rate, but a bit stronger.

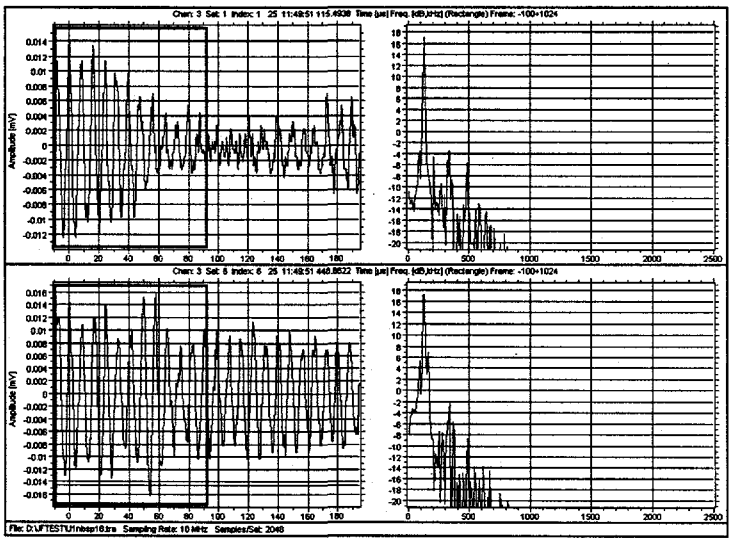

Figure 34. Narrowband sensors flow rate: 18 gpm.

At a flow rate of 19 gpm, a modulated signal appears in all three channels as shown in Figure 35.

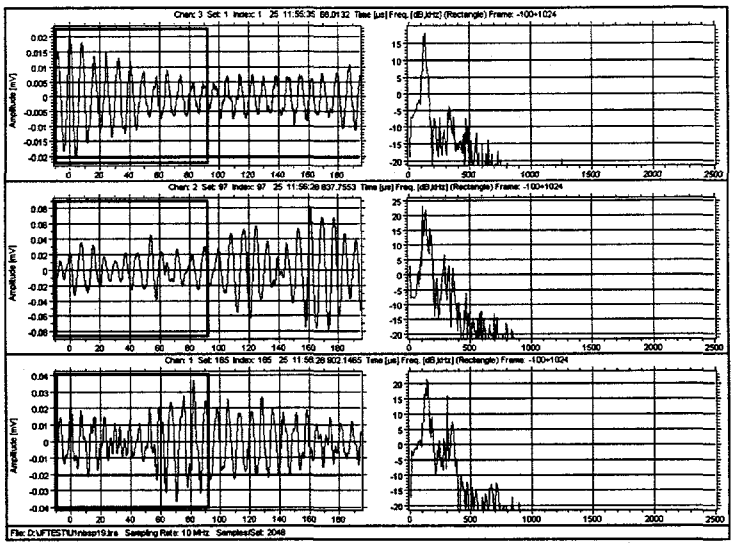

Figure 35. Narrowband sensors flow rate: 19 gpm.

At a flow rate of 20 gpm, the signatures are similar to those at 19 gpm as seen in Figure 36. At 20 gpm, the cavitation nozzle was beginning to crackle audibly.

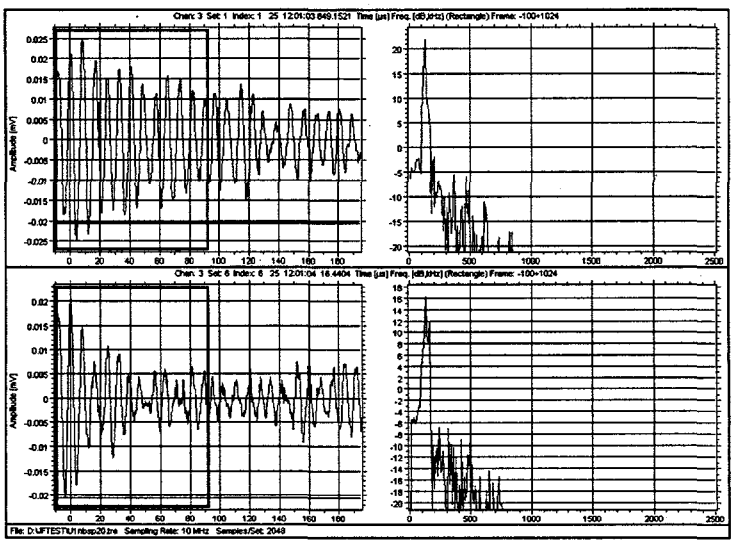

Figure 36. Narrowband sensors flow rate: 20 gpm.

At a flow rate of 25 gpm, captured events were decaying "chirp down" signals, as shown in Figure 37. At 25 gpm, the cavitation nozzle was crackling very loudly.

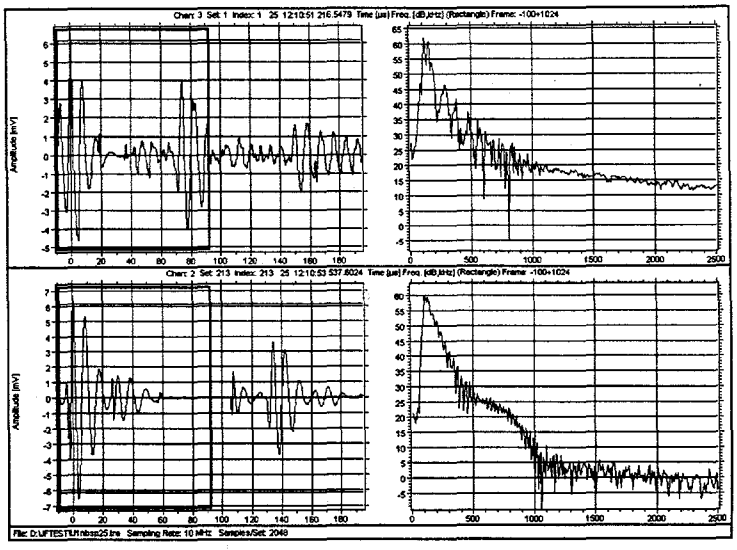

Figure 37. Narrowband sensors flow rate: 25 gpm.

At a flow rate of 30 gpm, captured events were decaying "chirp down" signals, as shown in Figure 38. At 30 gpm, the cavitation nozzle was crackling very loudly.

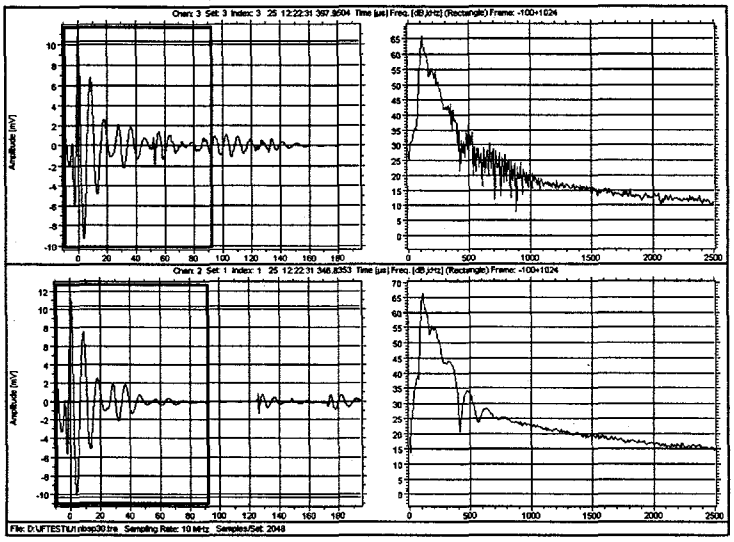

Figure 38. Narrowband sensors flow rate: 30 gpm.

The preceding data were captured by starting at zero-flow and incrementing upward. In order to observe the suspected hysteresis effect, the following data were captured at 19 gpm and then characterized to determine distinguishing features. At this flow rate, only two decaying "chirp down" signals were seen in Channel 2. In Channels 2 and 3, the modulated signal was quite common. Only one event was captured in Channel 1 with the widest throat diameter. Major features are shown in Figure 39.

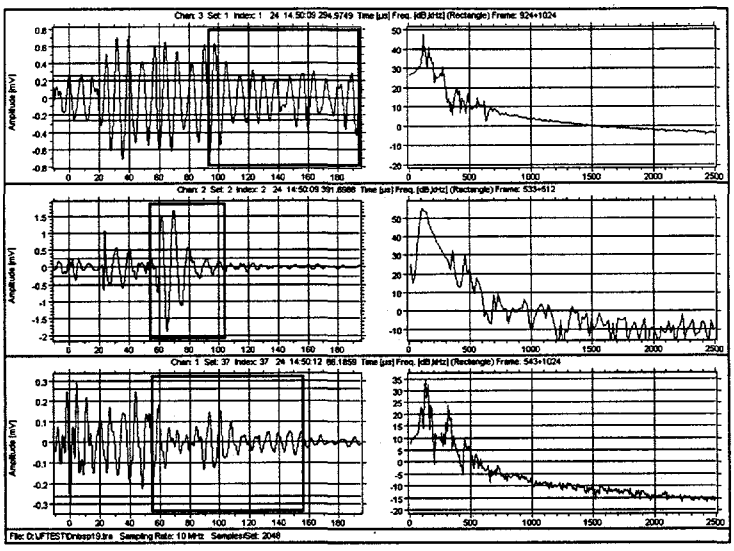

Figure 39. Narrowband sensors flow rate: 19 gpm.

At 18 gpm both chirps and modulated signals are noted as shown in Figure 40.

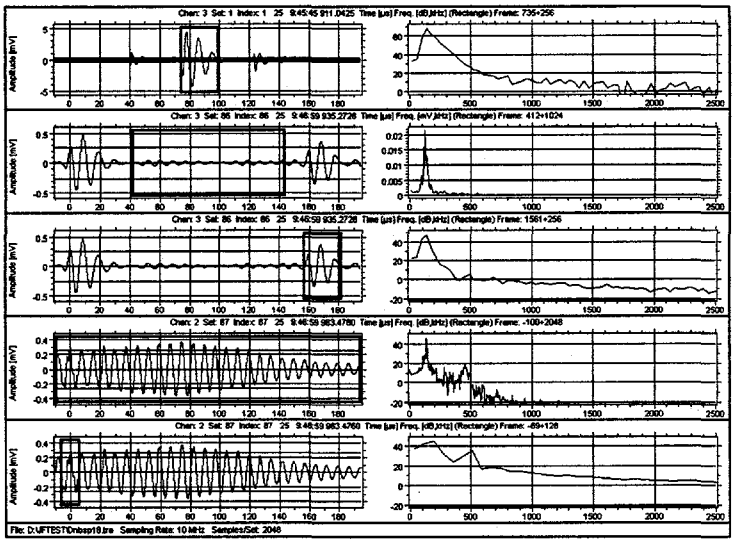

Figure 40. Narrowband sensors flow rate: 18 gpm.

At 17 gpm no captured events were decaying "chirp down" signals. All 99 signatures were captured in Channel 3. All were of the modulated form shown in Figure 41.

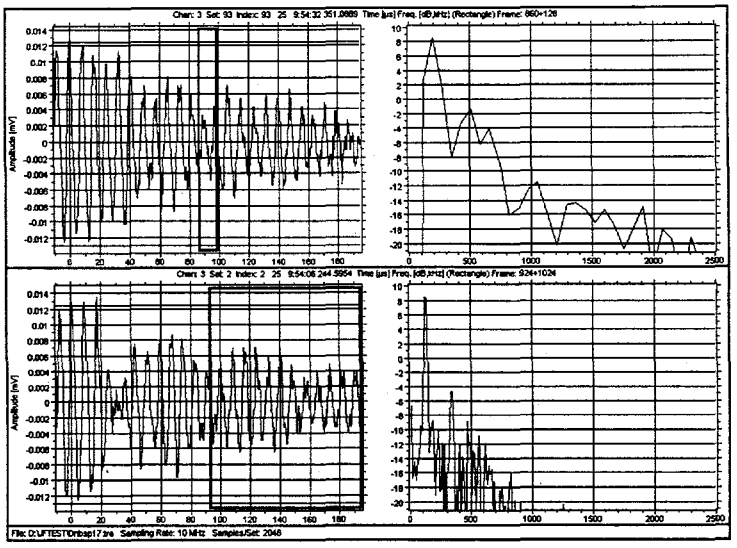

Figure 41. Narrowband sensors flow rate: 17 gpm.

At 16 gpm no captured events were decaying "chirp down" signals. All 100 signatures were captured in Channel 3. All were of the modulated form shown in Figure 42.

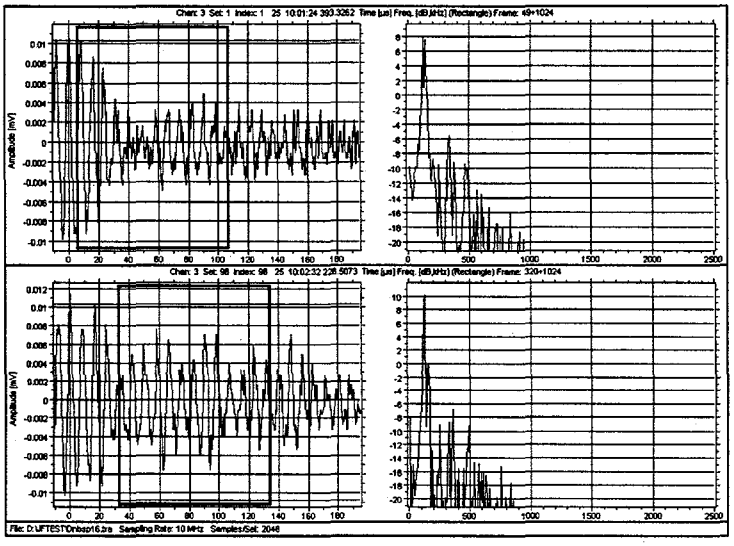

Figure 42. Narrowband sensors flow rate: 16 gpm.

At 15 gpm, 944 signatures were captured, at least some in all three channels. All were of the modulated form shown in Figure 43.

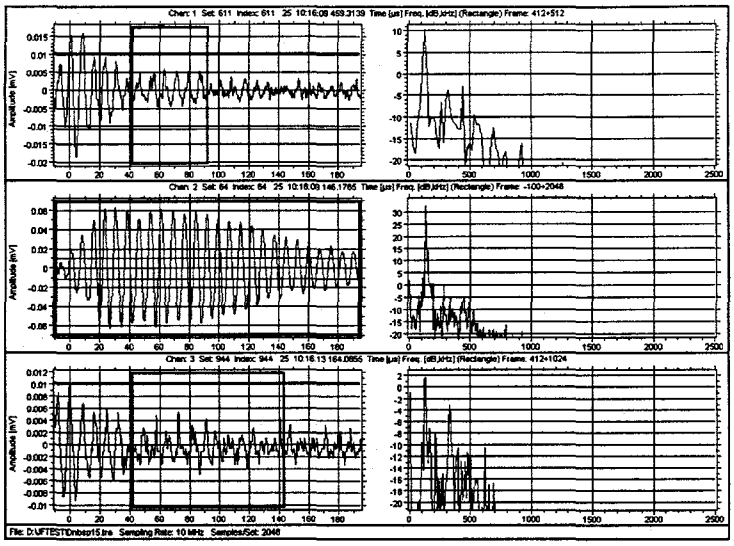

Figure 43. Narrowband sensors flow rate: 15 gpm.

At 14 gpm, 949 signatures were captured, at least some in all three channels. All were of the modulated form shown in Figure 44.

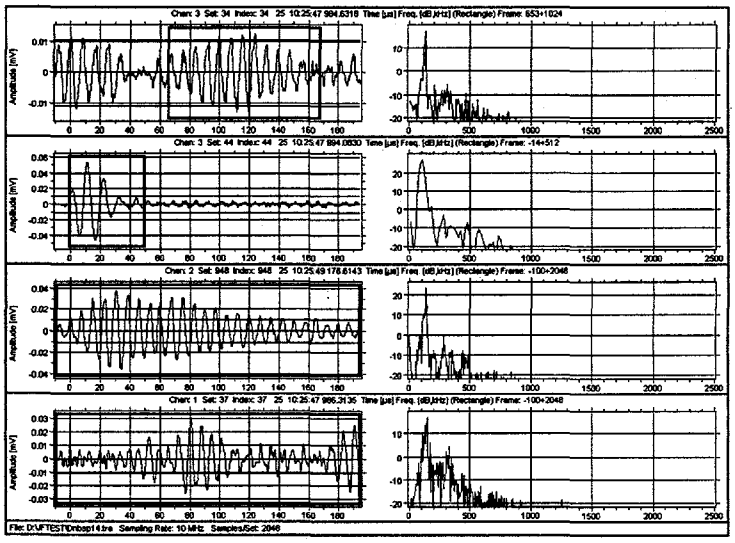

Figure 44. Narrowband sensors flow rate: 14 gpm.

At 13 gpm, 108 signatures were captured, at least some in all three channels. The event shown in the middle frame of Figure 45 (Channel 3) is the only event that does not look like simple sensor noise.

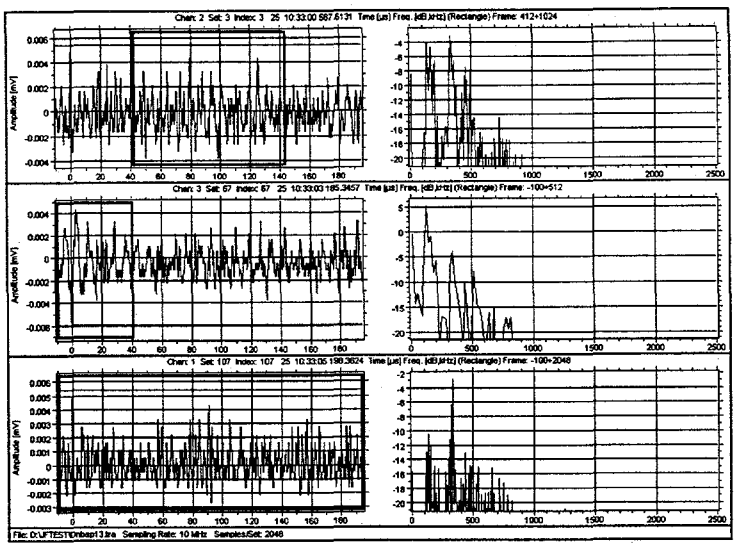

Figure 45. Narrowband sensors flow rate: 13 gpm.

At 12 gpm, 110 signatures were captured. As shown in Figure 46, they are indistinguishable from electronic noise.

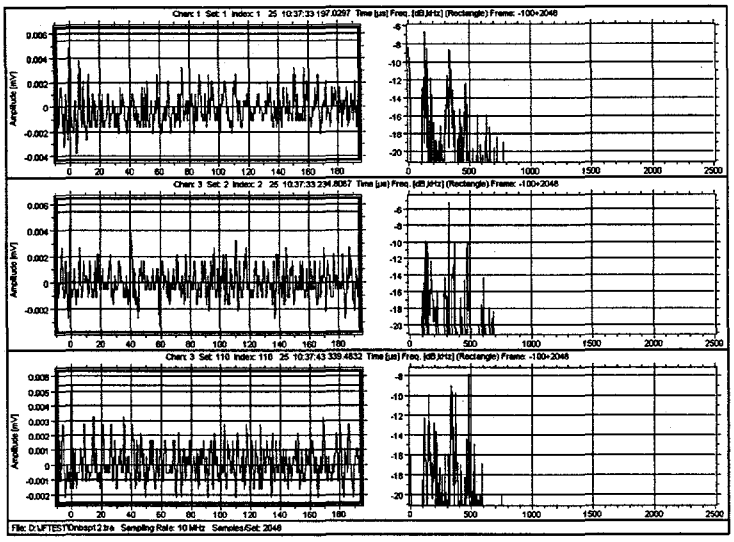

Figure 46. Narrowband sensors flow rate: 12 gpm.

The hysteresis effect seems less noticeable with the narrowband sensors than the broadband sensors. With the narrowband sensors, the eyeball analysis suggests that as the flow rate was incremented, there was only noise at 12 gpm, a hint of nonrandom activity at 13 gpm, quite noticeable signatures at 14 gpm, and ever strengthening signatures at 15 gpm and above. As the flow rate was decremented, there were noticeable signatures at 14 gpm, only a hint of nonrandom activity at 13 gpm, and only sensor noise at 12 gpm and below.

Note that various other signatures were captured. Those shown in this report are representative.

Preliminary Experimental Analysis

Generic Probability Function for Integration Over Location Parameters

Bayesian parameter estimation describes the best estimate of the description of the signal as the weighted sum of several model functions. Its amplitude, or linear parameter, gives the relative contribution of each model function to the overall model. In addition, within each model function, there may be one or more nonlinear parameters. In this technique, the distinguishing feature of a physical effect is the list of model functions and their parameters. As described previously, this general expanded concept of a "process feature vector" is the defining element of the CD-CBM paradigm.

There are as many amplitude parameters as model functions. But the nonlinear parameters are specific and must be searched for. All the nonlinear parameters are included in the parameters argument of the probability function; the amplitude parameters are implicit in the number of model functions in the model (the model's dimensions). The time or sampling points is assumed to consist of a sequence of regularly spaced integers from 1 to the length of the data set. If we wish to scale the sampling points, simply include the scale factor as a (known) nonlinear parameter. Thus, the model for a single oscillatory term might be

$$\{1, \cos(\omega t), \sin(\omega t)\} \text{ or } \{1, \cos(2\pi\omega t\kappa), \sin(2\pi\omega t\kappa)\}, \tag{12}$$

where κ is a scaling factor that takes the integer samples represented by t to microseconds and ω the frequency in MHz. In the first expression, ω is the frequency in radians. Consider the chirp model

$$\{1, \cos(2\pi\omega t\kappa+\alpha\kappa^2t^2), \sin(2\pi\omega t\kappa+\alpha\kappa^2t^2)\}. \tag{13}$$

Here, there are three explicit nonlinear parameters (α, κ, ω) and three implicit amplitude parameters. One of the nonlinear parameters is known, namely κ, the time-scale parameter. The two unknown parameters are α and ω, leading to a two-dimensional search or optimization problem in the ω, α-plane. Generally, if there are m unknown nonlinear parameters, the problem becomes a search in an m-dimensional space for the peak of the likelihood function. Should this prove too much of a computational burden, individual nonlinear parameters may be removed by integration in the usual manner. However, this may prove more difficult than a high-dimensional search.

Log likelihood is the log of the Student-t distribution. This assumes integration over all the linear model parameters. The Student-t is computed from the projection of the data onto the orthogonalized model, which should be the same number as the projection of the data onto the model and the inner product of the data vector with itself as

$$S_t = \left[1 - \frac{<d,m>}{<d,d>}\right]^{(M-N)/2}. \tag{14}$$

The projection of the data onto the model is <d,m> and <d,d> is the projection of the data onto itself. The number of functions in the model is represented by M, and N is the number of samples in the vector.

A typical example of the time-domain signature of a cavitation event seen in the AE data is shown in Figure 47. These types of signatures occur very frequently at high flow rates (thousands of instances per second at flow rates above 20 gpm). This is a particularly clean instance of the many observed at 30 gpm and is used to derive the cavitation signature event model. The amplitude is normalized to 1 at the peak value of the signature. The time-axis is in units of μ sec.

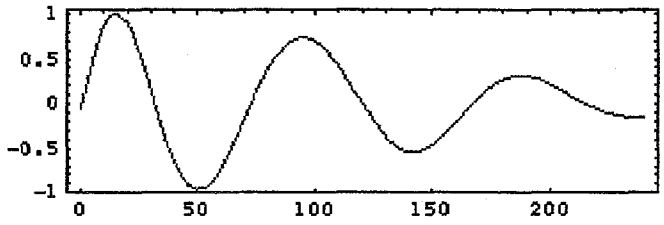

Figure 47. AE signature at 30 gpm.

The logic in developing the model-based descriptor is to find the most *reasonable* fit to the data that is consistent across the process and describes the known physics. Based on this, the first model chosen was a chirped undamped sinusoid. The assumed model is:

$$\{(\cos(\omega t\kappa+\alpha\kappa^2t^2), \sin(\omega t\kappa+\alpha\kappa^2t^2)\}. \quad (15)$$

Assume κ =1. Bayesian analysis computes the most probable nonlinear parameter values are α = 0.000813126066 098684319 and ω = 0.0841735989101785264. As shown in Figure 48, this does not provide an especially good fit to the data.

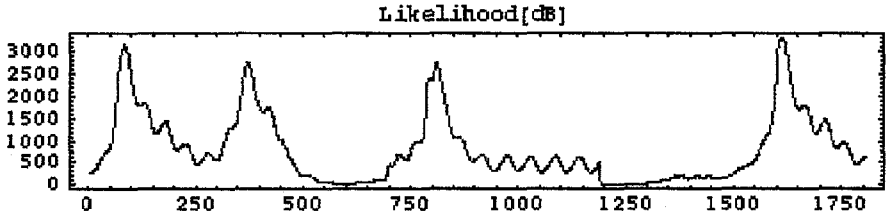

Figure 48. Fitted undamped chirp model compared to observed data.

The next step was to fit a chirped damped sinusoid to these data. The model is:

$$\{e^{-t}\cos(\omega t\kappa+\alpha\kappa^2t^2), e^{-t}\sin(\omega t\kappa+\alpha\kappa^2t^2)\}. \quad (16)$$

Assuming that κ=1, Bayesian analysis computes the most probable nonlinear parameter values are ω = 0.0877091, α = -0.000923205 and γ = 0.00553404. As shown in Figure 49, this provides a very good first order fit to the data. The damped chirp model is used in subsequent analyses.

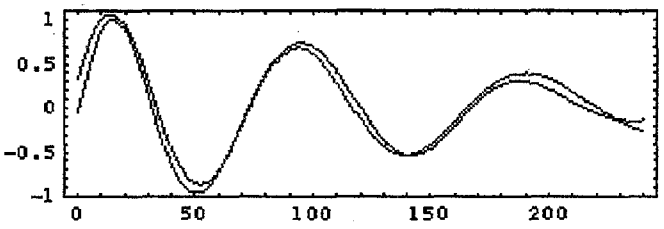

Figure 49. Fitted damped chirp model (red) compared to observed data (blue).

Consider a typical frame of data captured at 30 gpm with the narrowband sensor. At this flow rate, severe cavitation is occurring. This observation is supported by the audible crackling emanating from the venturi chamber. Figure 50 shows approximately 2000 μ seconds of data with maximum amplitude of approximately 20,000 μV.

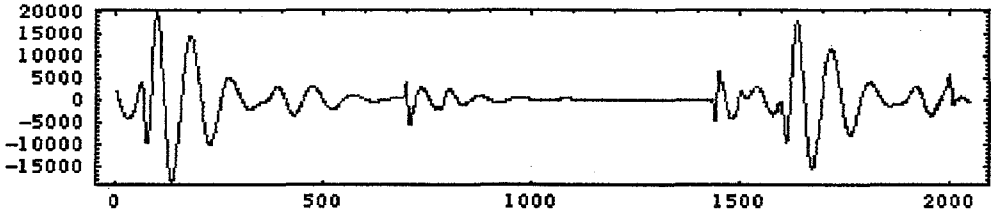

Figure 50. Several cavitation events at 30 gpm.

Likelihood is computed for each continuous set of 240 data points in the data as the model (used as a matched filter) is swept forward one sample at a time. The nonlinear parameters and then the linear parameters are calculated for the model and the goodness of the fit is determined by computing the log (likelihood) in dB. As shown in Figure 51, the signature of Figure 50 includes four events that are very likely damped chirp events.

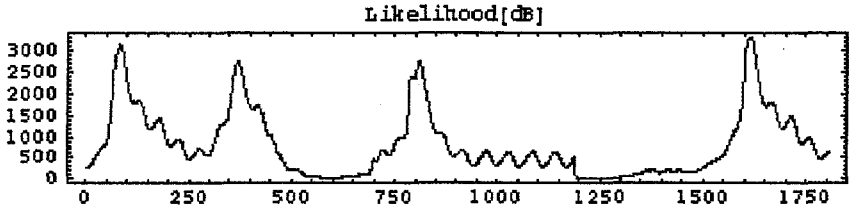

Figure 51. Likelihood of damped chirp events in the signature in Figure 50.

The four most likely events identified in Figure 51 and extracted from Figure 50 (blue), corresponding model (red) and their nonlinear parameters (ω,α,γ) are shown in the four plots of Figure 52. Amplitude of each event is shown in μV and time in μ sec. Two events are very strong and two are an order of magnitude weaker. It is noteworthy that the two weak events do not have significantly less likelihood than the two strong events.

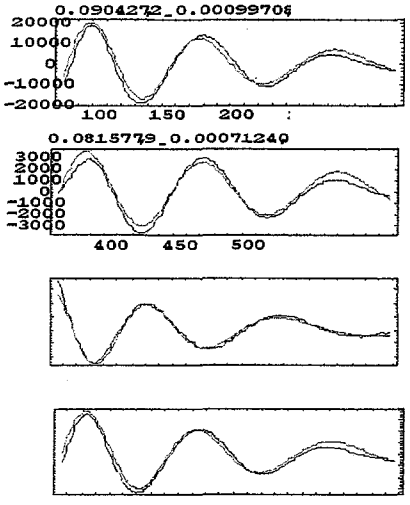

Figure 52. Four likeliest events in Figure 50.

Consider, now, a flow rate of 20 gpm where the cavitation is still audible. Approximately 6 milliseconds of time from this flow regime are shown in Figure 53. The likelihood of events described by the damped chirp model is shown in Figure 54. Note that the amplitude of the events is typically weaker by a factor of 5 compared to the events at 30 gpm. However, the log likelihood measures are still in the neighborhood of 3000 dB. The important conclusion is that despite the fact these events are substantially weaker than those at 30 gpm, they are no less likely to be detected by the damped chirp model. Similar results are seen for flow rates down to 18 gpm.

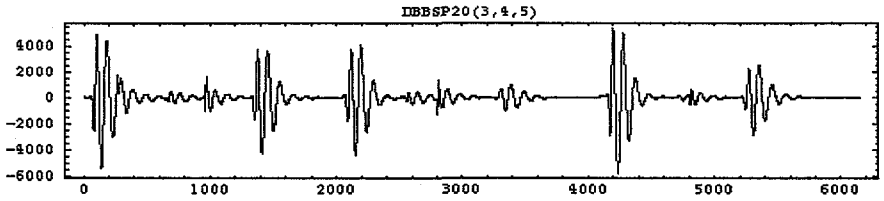

Figure 53. Several cavitation events at 20 gpm.

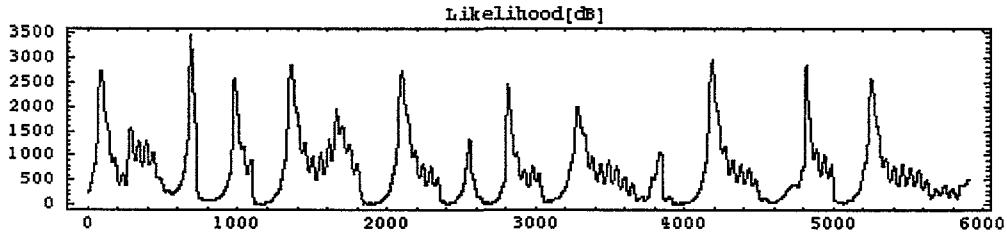

Figure 54. Likelihood of damped chirp events in the signature in Figure 53.

At flow rates below 18 gpm, cavitation (damped chirp features) is a rare occurrence. As Figures 55 and 56 show, a typical data set collected at 17 gpm is practically indistinguishable from the electronic noise of the experimental setup. [See Figure 57 - Note: The noise floor of the electronics is 1 μV root mean square (rms).]

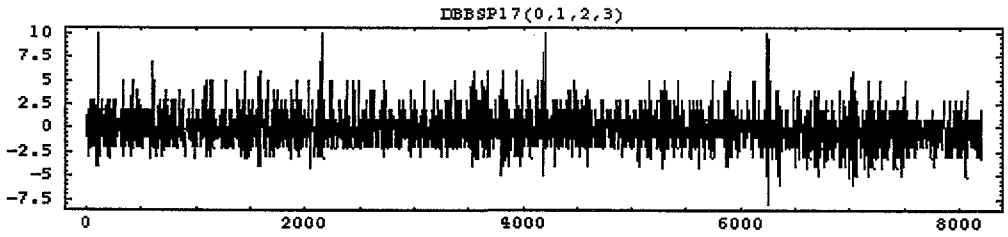

Figure 55. Typical data set at 17 gpm.

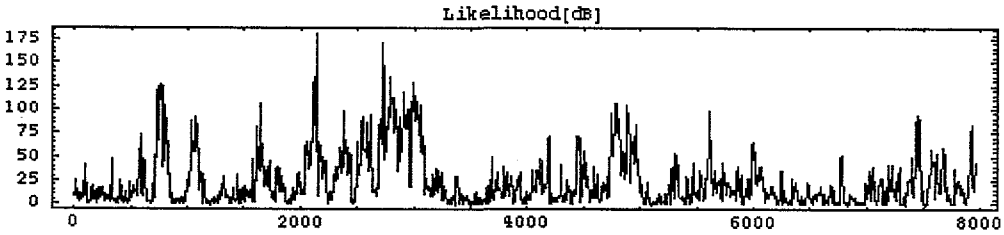

Figure 56. Likelihood of damped chirp events in the signature in Figure 55.

Compare Figures 55 and 56 with Figures 57 and 58. Figure 57 is a typical time domain signature with the sensors mounted on the venturi section but with zero flow through the flow loop. This is the AE signature of the noise from the environment plus the experimental apparatus itself. As seen in Figure 58, if the log likelihood measure is below 750, it is very unlikely that a damped chirp feature is present in the data.

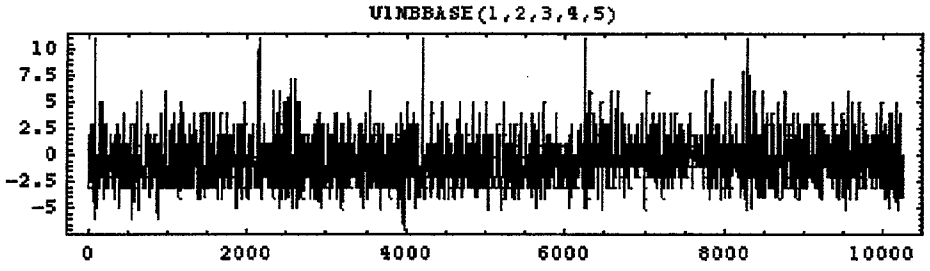

Figure 57. Typical data set at zero flow.

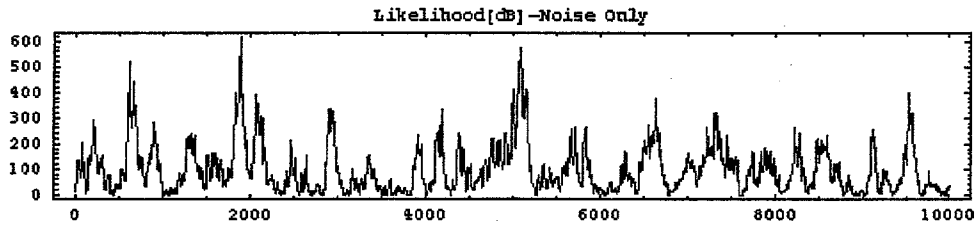

Figure 58. Likelihood of damped chirp events in the signature in Figure 57.

Although damped chirps are rare at 17 gpm, they do occasionally occur. Figure 59 (time domain shown above, likelihood shown below) shows the only event captured at 17 gpm with the broadband sensors that does not look just like noise. Two bursts are apparent in the time domain data, a stronger burst near the beginning and a weaker one just after the strong one. Both are only a little stronger than the background noise.

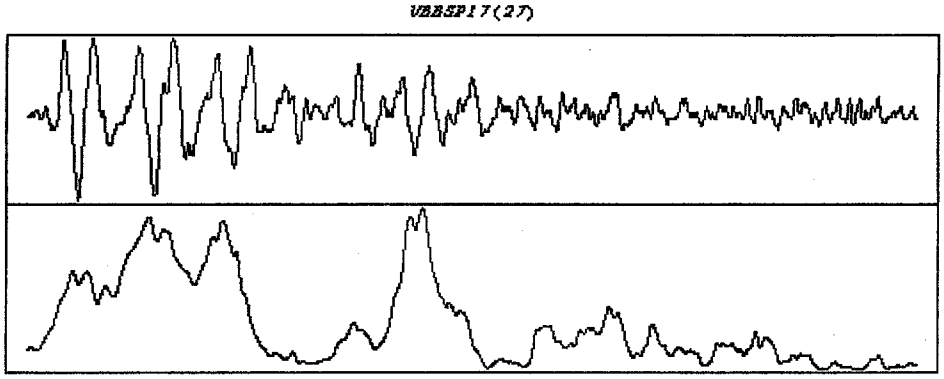

Figure 59. A possible damped chirp at 17 gpm.

Figure 60 shows more details of the log likelihood plot. It is noteworthy that the weaker burst between times 700 and 900 is more likely to be a damped chirp than the stronger burst between times 200 and 400. If the "threshold of cavitation" is between 17 and 18 gpm, it is possible the very weak damped chirp (amplitude on the order of 10 μV)

in the 17 gpm data is a precursor to the very strong damped chirp (amplitude on the order of 10 mV) signature in the data at 18 gpm and above.

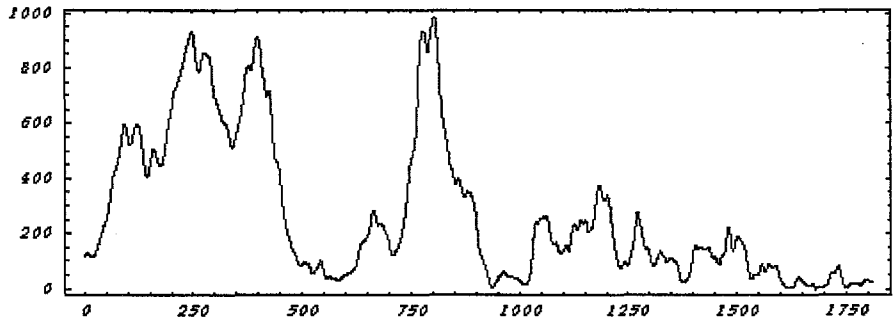

Figure 60. Log likelihood of damped chirp at 17 gpm.

Comparing the 17 gpm data with the zero flow data, it appears that one way to distinguish between the presence and absence of damped chirps is to use a log likelihood threshold of 750 as a decision point. The damped chirp appears to be a cavitation signature. Weak damped chirps (amplitudes of approximately 10 μV with this setup) with a high log likelihood (greater than 750) appear to be a useful cavitation precursor.

A bit of interpretation of the data yields some useful guidance at this point. The dominant frequencies of the damped chirps are in the range of $0.08 <= \omega <= 0.1$ radians. The sampling rate is 10^7 samples per second, meaning that the frequency of π corresponds to 5 MHz. The underlying dominant frequency of the physical chirps is in the range of 127-159 kHz. This is well within the flat response range of the broadband AE sensors. It is also in the resonance peak of the narrowband sensors whose sensitivity in the resonant band tends to be 5-15 dB greater than the sensitivity of the broadband sensors. This suggests that at flow rates below 17 gpm, occasional weak high-likelihood damped chirps will be seen with the narrowband sensors.

For example, consider a data set observed at 14 gpm with the narrowband sensors (Figure 61 - time domain shown above, likelihood shown below). Note that the two bursts most likely to be damped chirps are barely stronger than the noise and that the matched filter does not show a strong response to the much stronger signal that is unlikely to be a damped chirp.

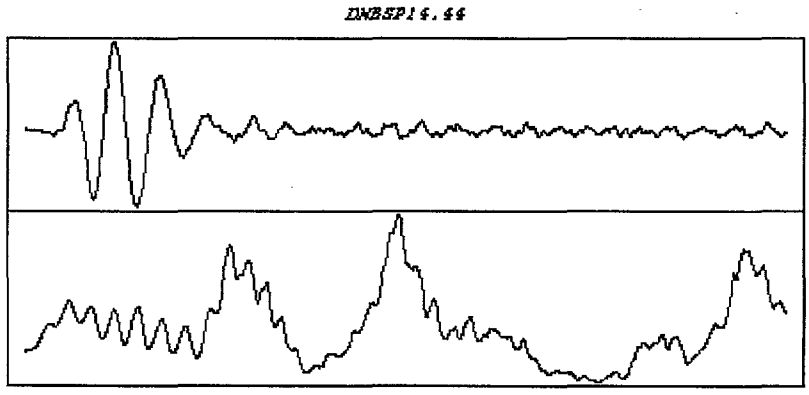

Figure 61. Likely damped chirps at 14 gpm in narrowband data.

Figure 62 shows more details of the log likelihood plot. It is noteworthy that three very weak damped chirps (amplitude below 10 μV) in the 14 gpm data are very likely to be damped chirps. It is also noteworthy that the strong burst at the beginning of the time domain signal is unlikely to be a damped chirp.

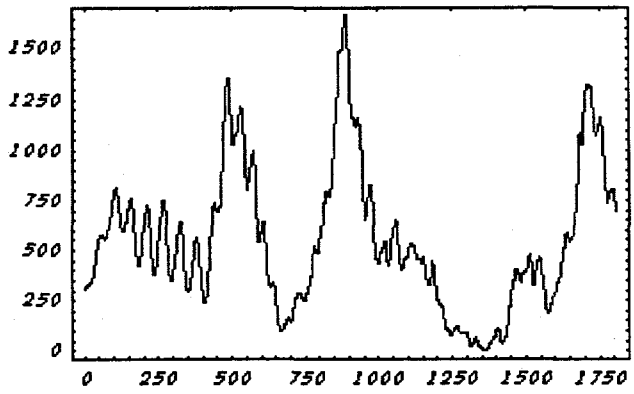

Figure 62. Log likelihood of damped chirps at 14 gpm.

Similar results are seen at 13 gpm. The events are rarer than at higher flow rates, but as shown in Figures 63 and 64, they do occasionally occur with high log likelihood. It is noteworthy that the damped chirp model detects one event with strong likelihood despite the fact that the physical signature is barely above the 1 μV rms noise floor of the experimental apparatus. Contrast this with Figures 61 and 62 in which it is clear that a very strong nonchirping signal does not produce a strong log likelihood measure.

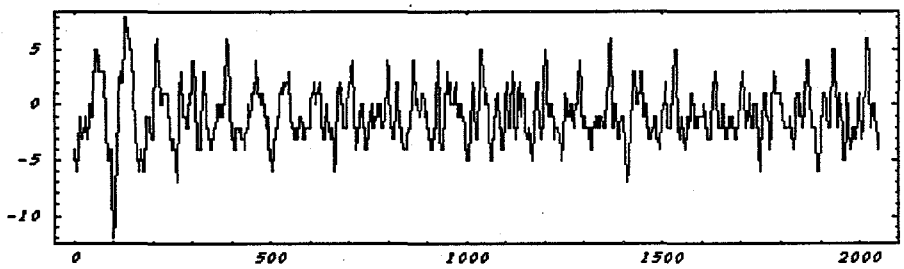

Figure 63. A rare damped chirp at 12 gpm (narrowband sensor).

The fact that a chirp appears in the severe cavitation and that the damped chirp appears to be a distinguishing feature of cavitation and its precursors is an especially convenient outcome. The chirped model is less easily fooled than some others are. For example, Figure 65 shows that a nonchirped model produces two strong likelihoods on the Figure 63 data, where the damped chirp only produces one.

The foregoing analysis is very preliminary and needs to be validated both by further analysis of the data collected in Phase I and by the collection of additional data. However, several preliminary conclusions appear to be reasonable. First, that a damped chirp AE signature seems to be a distinguishing feature of cavitation. Second, above the "threshold of cavitation" strong damped chirps are common occurrences. Third, below the "threshold of cavitation" weak damped chirps are rare (but not nonexistent) occurrences. Fourth, the amplitude of the damped chirps drops abruptly at the "threshold of cavitation," consistent with the concept that the inception of cavitation is a catastrophic bifurcation. Fifth, damped chirps are easy to detect and hard to confuse with other signatures when Bayesian parameter estimation is used. Sixth, at flow rates well below the threshold of cavitation, occasional damped chirps are observed with weak amplitudes (virtually indistinguishable from noise by the eye), but high log likelihood measure.

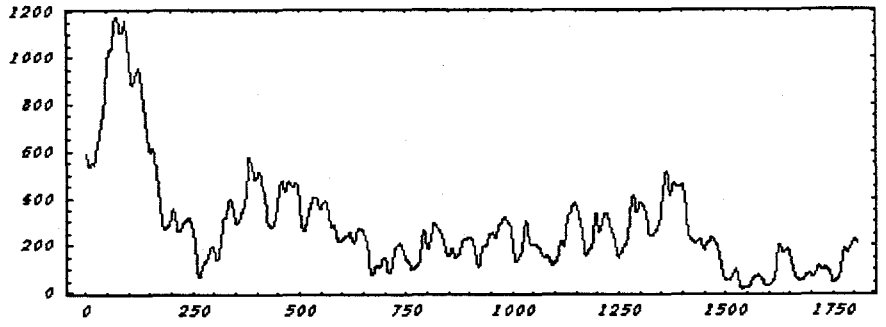

Figure 64. Likelihood of damped chirp events in the signature in Figure 63.

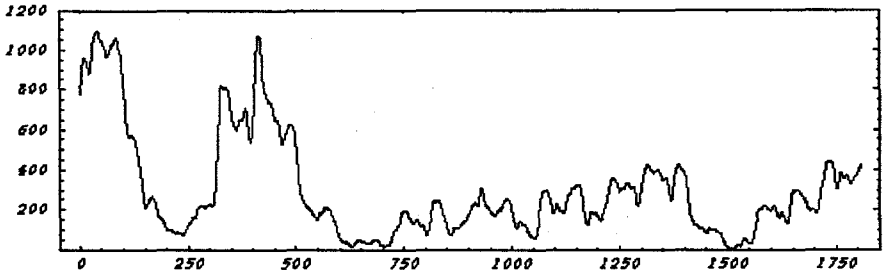

Figure 65. Likelihood of nonchirp events in the signature in Figure 63.

These conclusions have utility in two aspects of cavitation detection. First, it appears that the sudden appearance of strong damped chirps in response to a small increase in flow rate is a strong and reliable indicator of the inception of cavitation. Second, weak damped chirps at low flow rates appear to be cavitation precursors. This suggests that the Bayesian-derived damped chirp may be well suited to be a model in the anticipation engine in a formal anticipatory system. These data and their Bayesian analysis illustrate the principle that a CD-CBM anticipatory model can be used on real-world data to anticipate catastrophic occurrences.

Conclusions

Preliminary Systems Analysis and Operational Survey

Our survey of the literature suggested that the most compelling demonstration of principle for CD-CBM could be accomplished through experimentally searching AE signatures for cavitation precursors.

Define and Develop Feature Vectors for Selected Pump

The distinguishing feature of each different cavitation state is a data structure consisting of the functional model of the AE, parameter list, and probability-of-fit measure for each state. There is a distinct data structure for each cavitation state. The states are laminar flow (no detectable cavitation features or precursors), impending cavitation (precursors present, but difficult to distinguish from instrument noise), incipient cavitation (cavitation features begin to rise above the noise), and severe cavitation (audible crackling from flow loop).

The feature vector's formal structure is

$$fv \Rightarrow [\ \langle f(x,t,)\rangle, \{\text{parameter list}\}, \text{confidence factor}],$$

with a specific entry as follows:

$$fv \Rightarrow [<e^{-\gamma t}\cos(\omega t\kappa+\alpha\kappa^2t^2),\ e^{-\gamma t}\sin(\omega t\kappa+\alpha\kappa^2t^2),\{\omega=0.008,\ \gamma=0.0056,\ \alpha=-0.0009\},\ cf=0.80]. \quad (17)$$

Develop and Deploy a Baseline Proof-of-Concept Context-Dependent Monitoring System

The proof-of-concept showed that the distinguishing features of impending, incipient, and severe cavitation are present in AE of each of these types of flows. These features were observed in the venturi chamber in the flow loop described above and are typically decaying oscillatory bursts with a downward chirp in frequency. The observed signatures are consistent with the "harmonic cascade" theory of cavitation inception.

By using this descriptor as the model-based reasoning kernel, the CD-CBM anticipatory engine controlled the flow loop at points in the state space adjacent to incipient cavitation. [Control was instantiated through manual manipulation of the flow loop.] The system was then forced into differing cavitation states and then returned to safe operations based on a simple integrated damaged model based on time and model parametric values.

Conclusions and Recommendations for Phase II Based on Findings

The short-term goal of Phase II is to refine the CD-CBM anticipatory engine specific to cavitation and show a proof-of-principle use in the ORNL flow loop. The idea is to configure the CD-CBM model and anticipatory kernel into a real-time, closed-loop configuration based on some economic performance index and anticipate and control the flow to reject any decision to move the system into a state of cavitation.

The major goal for Phase II is to look directly at the nonlinear differential equation that governs the cavitation process, and using Bayesian analysis, derive the nonlinear differential equation and the relevant parameters for the given experiment. The interpretation of the experimental data can then be made by numerical solution of the nonlinear differential equation and will not require the simplifying assumptions that are necessary to guess an approximate solution and then trying to fit the parameters to it. This is in contrast to Phase I where the approach was to fit experimental data to guessed solutions of the differential equation. Another major goal of Phase II is to deploy the system in a laboratory environment and run operational scenarios on a pump and then extend this to an operational demonstration on a Navy ship.

REFERENCES

[1] Terry Wireman, *Computerized Maintenance Management Systems*, Industrial Press, New York, 1994.
[2] R. H. Green and D. A. Casada, *Detection of Pump Degradation*, NUREG/CR-6089, 1995.
[3] John H. Williams, Alan Davies, and Paul R. Drake, *Condition-based Maintenance and Machine Diagnostics*, Chapman and Hall, London, 1994.
[4] R. Rosen, *Anticipatory Systems: Philosophical, Mathematical, and Methodological Foundations*, Pergammon Press, Oxford, 1985.
[5] Dalhousie University Web Site, http://www.ced.tuns.ca/courses/1998/03/dt202.html.
[6] Christopher E. Brennen, *Hydrodynamics of Pumps*, pp. 74-76, Oxford University Press, Oxford, 1994.
[7] Ibid., p. 76.
[8] Ibid., pp. 89-90.
[9] Ibid., p.78.
[10] Ibid., pp. 92-93.
[11] Christopher E. Brennen, *Cavitation and Bubble Dynamics*, pp. 34-37, Equation 2.12, Oxford University Press, Oxford, 1995.
[12] Ibid., pp. 43-48.
[13] Brennen, *Hydrodynamics*, pp. 99-104.
[14] Brennen, *Cavitation*, pp. 79-80.
[15] Brennen, *Hydrodynamics*, pp. 108-111.
[16] Brennen, *Hydrodynamics*, pp. 111-118, Equations 6.14 and 6.15.
[17] S. Kumar and C. E. Brennen, "Some Non-Linear Interactive Effects in Bubbly Cavitation Clouds," *Journal of Fluid Mechanics*, Vol. 253, pp. 565-591, 1993.
[18] Brennen, *Cavitation*, pp. 83-91.
[19] Ibid., pp. 193-201.
[20] Brennen, *Cavitation*, pp. 182-187.
[21] Ibid., pp. 188-193, Equation 6.72.
[22] L. d'Agostino, C. E. Brennen, and A. J. Acosta, "Linearized Dynamics of Two-dimensional Bubbly and Cavitating Flows Over Slender Surfaces," *Journal of Fluid Mechanics*, Vol. 192, pp. 485-509, 1988.
[23] G. D. Neill, R. L. Reuben, P. M. Sanford, E. R. Brown, and J. A. Steel, "Detection of incipient cavitation in pumps using acoustic emission," *Proceedings of the Institution of Mechanical Engineers*, Part E, Vol. 211, pp. 267-277, 1997.
[24] L. Bretthorst, *Bayesian Spectrum Analysis and Parameter Estimation*, pp. 1-5, Springer-Verlag, Berlin, 1988.

DISTRIBUTION

INTERNAL

1–5. G. O. Allgood
6. W. B. Dress Jr.
7. S. W. Kercel
8. C. R. Brittain
9. J. M. Jansen Jr.
10. R. A. Kisner
11. D. W. McDonald
12. R. W. Tucker Jr.
13–15. Laboratory Records
16. Central Research Library
17. ORNL Patent Section

EXTERNAL

18–27. Mike Hoban, AEPTEC Microsystems, Inc., 15800 Crabbs Branch Way, Suite 300, Rockville, MD 20855